

Gonzalo Alvarez Morales

# **BIOPHOTONIC SCAFFOLDS FOR DRUG RELEASE USING NIR EXCITATION**

Tampere University  
Master thesis  
04/2020

# ABSTRACT

**Gonzalo Alvarez Morales:** Photosensitive drug loaded scaffolds with upconversion

Master thesis, 57 pages

Tampere University

Material's science and engineering.

05/2020

Master's Degree Program in Materials Science and Engineering, MSc

Major: Photonic materials

Supervisor: Dr. Laetitia Petit Dr. Jonathan Massera & Dr. Mikko Hokka (Associate Professors)

Keywords: Bioactive glass, Borosilicate, DSC, Upconversion, pH, SBF, scaffold, sintering, DDS.

---

Drug delivery systems (DDS) allow for precise control of the concentration of a drug in the organism over space and/or time. If loaded with the drugs before implantation, DDS could be engineered to release the drug under external stimulus. This stimulus could be light at 980nm which can penetrate the skin. This biophotonic DDS could then fight infections locally. Such DDS need to be fabricated from bioactive glasses which react when pumped at 980nm. Such glasses are capable of firm bonding with the surrounding tissues by developing bone-like hydroxyapatite (HA) layers when reacting with physiological fluids.

This thesis is focused on the development of the glass which will be used for the fabrication of the DDS: The glass of investigation is glass S53P4 (commercially available as BonAlive®) derivative from 50% SiO<sub>2</sub> substitution (B50), which shows a faster dissolution, and faster conversion into HA than S53P4 glass. Er<sup>3+</sup> & Yb<sup>3+</sup> ions and NaYF<sub>4</sub>:Er<sup>3+</sup>,Yb<sup>3+</sup> nanocrystals (NCs) were added in the bioactive glass so it can exhibit upconversion luminescence properties under 980nm pumping.

The development of upconverting glasses with the possibility to be sintered into highly porous scaffolds with high upconversion is first discussed. The glasses with the composition 95.5B50-0.5Er<sub>2</sub>O<sub>3</sub>-4Yb<sub>2</sub>O<sub>3</sub> (in mole %) and with the composition 98%B50-2% NaYF<sub>4</sub>:Er<sup>3+</sup>,Yb<sup>3+</sup> (wt.%) were found to be the most promising glasses for the fabrication of the scaffolds which are not only bioactive but also exhibit green light under 980nm pumping. Scaffolds were processed using the burn off method. They possess the appropriate level of porosity and exhibit upconversion. However, crystallization occurred during the sintering leading to some changes in the shape and intensity of the upconversion. The mechanical properties of the modified scaffolds were comparable to those of the B50 scaffold.

Scaffolds with 60-75% porosity were immersed in SBF for up to 336h. We found that they have a slower dissolution rate than the base glass but maintained an acceptable dissolution rate. The possibility to use the developed scaffolds in DDS using external near infrared excitation as a control signal is finally discussed in this thesis.

# PREFACE

I would like to thank my colleges who have helped me with the little hardships over course of the thesis and providing a collaborative environment where favors were interchanged, specially Nirajan, who shared an office with me, and answered all questions I had along the project. I would like to specially mention my supervisors Mikko Hokka, Jonathan Massera, and mainly Laetitia Pettit, who not only taught me how to do the different laboratory procedures, but also guided me during this period.

Special thanks should be given to my Family who not only financially supported me to be able to do this project, but most importantly provided an invaluable psychological support that allowed me to prevail against the hardships over these months with a positive view.

Lastly, I would like to mention my friends, both the ones here in Finland, and the ones back in Spain, who have provided their unconditional support, without which I don't think I could have done it.

Thank you,

Tampere, 14 April 20209

Gonzalo Álvarez Morales

# CONTENTS

1.	Introduction & objectives .....	1
2.	Theoretical background.....	3
2.1	Glass .....	3
2.1.1	Photonic glasses.....	4
2.1.2	Biomaterials .....	7
2.1.3	Bioactive glasses .....	8
2.2	Bioactive scaffolds.....	9
2.2.1	Materials used for the fabrication of scaffolds .....	10
2.2.2	Requirement for glass scaffolds and their fabrication process.....	11
2.2.3	Borosilicate scaffold .....	12
2.3	Drug delivery systems .....	13
2.3.1	Localized drug delivery systems .....	14
2.3.2	Proposed localized drug delivery system .....	15
3.	Materials and methods.....	17
3.1	Material's preparation .....	17
3.1.1	Glass preparation.....	17
3.1.2	Scaffolds sintering.....	17
3.1.3	Photocleavable molecules .....	19
3.2	Material's properties .....	20
3.2.1	Physical properties.....	20
3.2.2	Thermal properties.....	20
3.2.3	Optical properties.....	21
3.2.4	Spectroscopic properties.....	22
3.2.5	Mechanical properties.....	23
3.2.6	Porosity measurement .....	23
3.2.7	In vitro testing .....	24
3.2.8	X-ray diffraction analysis .....	24
3.2.9	Scanning electron microscope .....	25
4.	Results and discussion .....	28
4.1	Preparation and characterization of scaffolds .....	28
4.1.1	Yb <sup>3+</sup> , Er <sup>3+</sup> doped scaffolds.....	28
4.1.1.1	Optimization of the Er <sub>2</sub> O <sub>3</sub> and Yb <sub>2</sub> O <sub>3</sub> content .....	28
4.1.1.2	Fabrication and characterization of the Yb <sup>3+</sup> , Er <sup>3+</sup> doped scaffolds	32
4.1.2	Scaffold preparation with NaYF <sub>4</sub> : Yb <sup>3+</sup> , Er <sup>3+</sup> nanocrystals .....	35
4.2	Photocleavage of molecules using NIR pumping.....	39
4.2.1	In vitro testing .....	40
4.2.2	Drug released using 980nm excitation .....	40
5.	Conclusions .....	43
Next steps outside of the scope of the project .....	44	
6.	References .....	45

# LIST OF FIGURES

Figure 2-1: Rare earths elements [Mi,20].....	4
Figure 2-2: Energy diagram photophysical effects in light amplification by stimulated emission of radiation (Laser) [Fi,20].....	5
Figure 2-3: Schematic of laser emission. [Ki,11].....	6
Figure 2-4: Simplified energy level diagram of $Er^{3+}/Yb^{3+}$ ions. Upwards arrows indicate excitation photons and downwards arrows stand for emission photons [Ol,98].....	7
Figure 2-5: Scheme of different biocompatibility degrees: biotolerance (a), bioinertness (b) bioactivity (c).....	8
Figure 2-6: Microstructures of bioactive glass scaffolds created by a variety of processing methods [Ra,11].....	9
Figure 2-7 Different bioactive glasses available [Fa,12].....	11
Figure 2-8:Hypothetical drug concentration profiles in the systemic circulation resulting from the consecutive administration of multiple doses of an immediate-release drug delivery system (A), A2, • • ) compared to the ideal drug concentration profile (B) required for treatment. [Yi,91].....	13
Figure 2-9:Classes of DDSs [Yi,91].....	14
Figure 2-10: Absorption spectrum of human skin [He,14].....	15
Figure 2-11: Modified schematic of the proposed DDS from [Zh,17].....	15
Figure 3-1: Ball milling mechanism. [Mio,04].....	18
Figure 3-2: PAI photoswitchable molecule [Ri,19].....	19
Figure 3-3: Absorption spectra of PAI after different irradiation (a) and absorbance over several irradiation cycles (b) [Ri, 19].....	19
Figure 3-4: Thermogram of a glass.[Ro,18].....	20
Figure 3-5: Schematic of a double beam spectrophotometer [Je,15].....	21
Figure 3-6: Schematic of upconversion, and proposed upconversion mechanism between $Yb^{3+}$ and $Er^{3+}$ . [Pa,16].....	22
Figure 3-7: $\sigma$ - $\epsilon$ curve of highly porous ceramic [Al,12] (a) and of B50 + 1.5%NCs (b).....	23
Figure 3-8: Sketch of XRD working principle [Ph,13].....	24
Figure 3-9: XRD set up in a $\theta$ - $2\theta$ configuration (fixed x-ray source) [Ep,16].....	25
Figure 3-10: Schematics of a SEM [Go,12].....	26
Figure 3-11: Typical EDS spectrum [Go,12].....	27
Figure 4-1: Picture of the borosilicate glasses prepared with different $Er_2O_3$ - $Yb_2O_3$ contents (mole %).....	29
Figure 4-2 Density as a function of $Er_2O_3$ (a), $Yb_2O_3$ (b) and total RE content (c).....	30
Figure 4-3: $T_g$ (a) an $T_x$ (b) as a function of $Er_2O_3$ and $Yb_2O_3$ content.....	30
Figure 4-4: Absorption spectrum of the 0.5-4 glass.....	31
Figure 4-5: Up conversion spectra of selected glasses.....	32
Figure 4-6: Porosity values of the different $Yb^{3+}$ , $Er^{3+}$ codoped scaffolds.....	33
Figure 4-7: Compressive strength curve of a doped scaffold.....	33
Figure 4-8: Upconversion spectra of scaffolds (a) and of the glass prior to and after sintering. (b).....	34
Figure 4-9: XRD pattern of the $Yb^{3+}$ , $Er^{3+}$ doped scaffold.....	35
Figure 4-10: Porosity and compressive strength curve of NCs containing scaffolds.....	35
Figure 4-11: Comparison between up conversion spectra of NC containing scaffolds before and after sintering.....	36
Figure 4-12 NCs alone UC spectrum prior to and after sintering.....	37

Figure 4-13 XRD pattern of the 10wg% NCs containing scaffolds and of the NCs alone.....	38
Figure 4-14: SEM pictures of the NCs scaffolds:.....	38
Figure 4-15: SEM image (a) and elemental EDS mapping (b) of the NCs containing scaffold .....	39
Figure 4-16: pH of the immersion solution (a) and scaffolds mass loss (b) of as a function of immersion time of in SBF. The undoped scaffolds are labelled as "B50", the $Er^{3+}$ , $Yb^{3+}$ , codoped scaffolds as "Doped", and the $NaYF_4: Yb^{3+}, Er^{3+}$ nanocrystals containing scaffolds as "NCs". A blank sample (only SBF) is also displayed, to show the variation in pH of the buffering solution, as a function of incubation time.....	40
Figure 4-17: Absorption spectrum of as received PAI molecule .....	41
Figure 4-18: Absorption spectrum of PAI solution in SBF irradiated with UV lamp from the top (a) and from the side (b) .....	41
Figure 4-19 Absorption spectrum of PAI solution in SBF after irradiation with green light .....	42

# LIST OF TABLES

Table 1: Density and thermal properties 29

Table 2: Absorption coefficients and cross-sections of the investigated glasses 31

## LIST OF SYMBOLS AND ABBREVIATIONS

0.5-4 glass: 0.5% Er<sub>2</sub>O<sub>3</sub> & 4% Yb<sub>2</sub>O<sub>3</sub> doped B50 glass.

0-0 glass: B50 glass

DSC: Differential scanning calorimetry

DDS: Drug delivery systems

NC: Nanocrystal containing scaffolds

PAI: Phthalimide-Azo-Iperoxo

RE Rare earth

SBF: Simulated body fluid

$\Delta T$ : Gauge of crystallization

T<sub>g</sub>: Glass transition temperature

T<sub>p</sub>: Crystallization peak's temperature.

T<sub>x</sub>: Temperature at onset of crystallization

UC Up-conversion

# 1. INTRODUCTION & OBJECTIVES

Together with the development of medical science, biology and engineering, there has always been an interest of merging their knowledge to create new methods and materials to improve medical treatments and reduce their complications. To improve live conditions of humans, various materials are being researched and innovated to be used in medicine. One of the main current focuses of research is biomaterials, which have been defined by Williams as “A biomaterial is a substance that has been engineered to take a form which, alone or as part of a complex system, is used to direct, by control of interactions with components of living systems, the course of any therapeutic or diagnostic procedure, in human or veterinary medicine” [Wi,09]

Biomaterials are a big topic that can be further classified depending on both their origin and their interaction with the body: i) bioactive materials: they can form a chemical bonding with the surrounding tissue; ii) bioinert materials: they don't react with the body, and iii) biotolerant materials: they are encapsulated by conjunctive tissue layer. This thesis focuses on the development of inorganic bioactive materials, specifically, on bioactive glasses. Bioactive glasses have been previously defined as a subset of the inorganic bioactive materials that is capable of reacting with physiological fluids to form firm bonds to bone through the development of hydroxy apatite (HA) layers, a main constituent of bone, as well as providing a proper surface interaction to collagen [He,71]. Since the creation of the first bioactive glass (Bioglass®) in 1969 by Larry Hench [He,71], research on bioactive glasses has grown exponentially, and novel glass compositions, manufacturing techniques and structures have been developed. Other alternatives have been tried to mix bioactive materials and photonics [Do,09]. However, not much research has been performed with the aim to combine this research with the photonics field. Biophotonics field has several promising qualities for the development of devices that can communicate fast and without invasive surgery. The device can be engineered to operate in a spectral range where the body is transparent to the signal, allowing external communication at the speed of light. In order to maximize the utility of the properties that photonics can provide, a drug delivery system was envisioned, that can be placed in a dormant state inside the host during a surgery as a substitute to the damaged tissue, but in case of detected infection, it can rapidly be activated and modulated to fight against it.

Before 1950, all drugs were made into either a capsule or a pill to release their loading immediately after contacting water, without any kind of control on the kinetics of the release [Yu,15]. In 1952, Smith Klein Beecham created the first controlled delivery, achieving a twelve hours long efficacy of the drug [Le,10]. During the first generation of drug delivery systems (DDS) (developed between 1950 & 1980), the different systems only allowed for a controlled or retarded release of the drug. Second generation (1980-2010), had a lower success rate in releasing products to the market, and suffered from an initial release spike during the first days, releasing almost of the drug, even if the effects were supposed to last for a couple months. Also, second generation suffered from problems in dealing with targeted treatments for tumoral cell using nanoparticles, which have not yet been successful. The third generation, which started in 2010, has tried to solve all the previous issues and found either long term release (several months between external dosage, targeted treatment or externally controlled dosage) [Yu,15].

This thesis focusses on the development of a new generation of DDS from newly engineered biophotonics glass-based scaffolds for drug release using external near infrared excitation as a control signal.

The main content of this thesis is divided into four different parts. First, in chapter two, a background introduction of the required fields for the understanding of this work is presented. General concepts in glass science, biomaterials, scaffolds and drug delivery systems is provided. A deeper insight to the specific areas of photonic and bioactive glasses, as well as scaffold and drug delivery system production is presented. This document follows with chapter three; whose purpose is to present and explain the methodology carried out during the experimental part of this thesis, along with explaining the preestablished knowledge about the main materials used during this thesis. To continue, chapter four describes the results obtained from the experimental procedures carried out during the development of the work, in addition to discussing the meanings and implications these results have. This chapter is divided into two different sections: 1) the production of the glasses, and sintering of the scaffolds are explained together with their mechanical and optical characterization and 2) the bio- and photo-response of the materials is analyzed. Finally, chapter five summarized the main conclusions obtained from this study and lists also the next steps which should be followed in order to properly supplement and continue this work.

## 2. THEORETICAL BACKGROUND

### 2.1 Glass

Glasses are a group of materials characterized by having amorphous solid state (lack of long-range order) and a glass transition temperature ( $T_g$ ). (Shelby 2005). The glass transition temperature of a glass is the temperature under which the material stops behaving as a liquid while still not crystallizing after a fast-enough cooling.

The process of glass forming from a liquid is called vitrification and this process is based on the reduction of the available energy and time for the material, locking it into a metastable state.

A glass is made by up to five different components: glass former ions, network modifiers, intermediate oxides, dopants and impurities. (Shelby 2005)

- **Glass former ions** are responsible for the creation of the backbone of the glass. This group includes  $\text{SiO}_2$ ,  $\text{P}_2\text{O}_5$  &  $\text{B}_2\text{O}_3$  just to cite a few and they create a network by joining the cations with bridging oxygens.
- **Network modifiers** are responsible to open and disrupt the network increasing the free volume. These component bond ionically to the bridging oxygens transforming them into non-bridging oxygens. Examples of these components are alkaline or alkaline-earth metal oxides. ( $\text{Na}_2\text{O}$ ,  $\text{K}_2\text{O}$ ,  $\text{CaO}$ , ...).
- **Intermediate oxides** are components that contribute in the formation of the network but cannot create a glass network by themselves. Example of these components are  $\text{Al}_2\text{O}_3$ ,  $\text{TiO}_2$  &  $\text{ZnO}$ .
- **Dopants** are components which do not change the glass structure when introduced in few mol%. They sit in the free volume and are added to the glass to alter some of its properties. Some examples are  $\text{Ag}_2\text{O}$  or rare-earth ions such as  $\text{Er}_2\text{O}_3$ ,  $\text{Yb}_2\text{O}_3$ .
- **Impurities** are components not desired in the glass and so they may alter some of the glass properties. Examples are contamination from the production process such as the crucible, furnace or the impurities from the raw materials and water (OH groups).

Glass materials are known since ancient times as the first glass production can be tracked back into 2500BC in Syria. The production was extended into other nearby civilizations of the time such as Mesopotamia and Egypt before spreading worldwide. But glasses are not just artificially made materials as vitreous materials can also be found in nature, such as obsidian, an igneous rock made by the fast cooling of lava from volcanoes. [Ru,19]

Glasses are known to be strongly affected by small alterations in their production due to their intrinsic metastable nature, as they don't relax to a minimum energy disposition (crystal) but are "frozen" into a midpoint while trying to adapt. The specific midpoint they are stuck into is determined by all the glass history.

Nowadays glass materials are used in multiple applications such as packaging, housing, automotive, electronics and energy production as well as photonics and medical technology, disciplines deeply related to the topic of this document.

### 2.1.1 Photonic glasses

Photonics is dealing with the photon generation and detection, as well as stimulated emission, photon frequency conversion and polarization change. This branch of science was born with the invention of the ruby laser in 1960, and the Photonics word was first used in 9th International Symposium on High Speed Photograph in 1970, when it was defined as “a systematic science concerning the photon as the information carrier”.

The development of photonics as well as the related fields of optics and opto-electronics still needs to explore new materials, in which glassy or amorphous materials are the important ones [Fu,06].

Photonic glasses are a branch of optical glasses defined as optically homogeneous glass, free from defects. They include several families such as laser glasses, nonlinear functional glasses and new photonic glasses (Photo-induced data storage glasses, photonic crystals, ...)

**Laser glasses** are glasses doped with laser active rare-earth (RE) ions, highlighted in Fig: 2-1.

H																	He
Li	Be											B	C	N	O	F	Ne
Na	Mg											Al	Si	P	S	Cl	Ar
K	Ca	Sc	Ti	V	Cr	Mn	Fe	Co	Ni	Cu	Zn	Ga	Ge	As	Se	Br	Kr
Rb	Sr	Y	Zr	Nb	Mo	Tc	Ru	Rh	Pd	Ag	Cd	In	Sn	Sb	Te	I	Xe
Cs	Ba	La-Lu	Hf	Ta	W	Re	Os	Ir	Pt	Au	Hg	Tl	Pb	Bi	Po	At	Rn
Fr	Ra	Ac-Lr	Rf	Db	Sg	Bh	Hs	Mt									
lanthanide series		La	Ce	Pr	Nd	Pm	Sm	Eu	Gd	Tb	Dy	Ho	Er	Tm	Yb	Lu	
actinide series		Ac	Th	Pa	U	Np	Pu	Am	Cm	Bk	Cf	Es	Fm	Md	No	Lr	

Figure 2-1: Rare earths elements [Mi,20]

These ions absorb pumped light which excites their electron into metastable levels and emit light when they relax by stimulated emission of radiation, an effect where a photon stimulates an excited atom to emit a photon coherent (same energy, momentum and phase) with the initial one (Fig: 2-2).

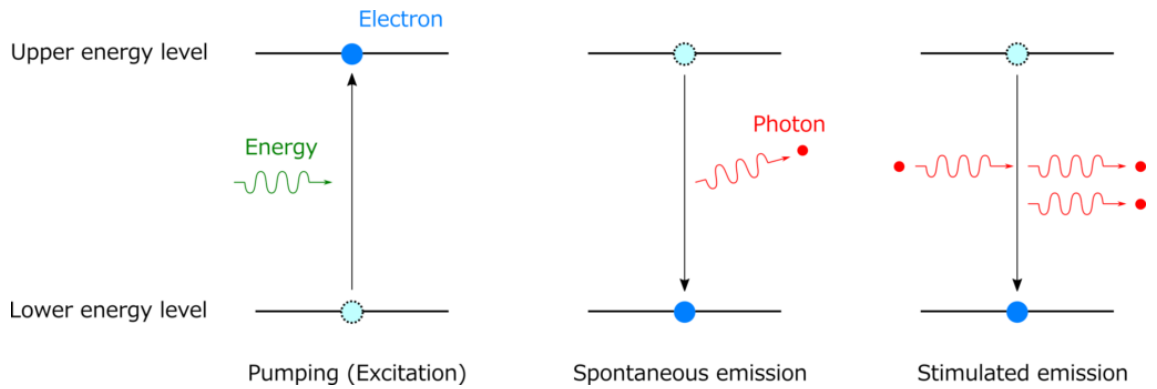


Figure 2-2: Energy diagram photophysical effects in light amplification by stimulated emission of radiation (Laser) [Fi,20].

This effect escalates quickly in the proper medium. By a proper control of the medium (population inversion, proper confinement of desired photons & elimination of undesired photons), a cascade of coherent photons can be created and directed into forming a beam.

As specified, lasing requires a population inversion, this is a key parameter as in order to promote stimulated emission over absorption, there is a requirement of having a more populated high energy level than ground level, this situation is called population inversion.

In order to produce large laser effect, a huge interaction between the lasered light and the material is required. This is usually obtained by confining the lasered light into a specific volume by the use of mirrors. The use of two mirrors, one perfect mirror, and one almost perfect one is the most common procedure to obtain laser effect, these mirrors are facing each other creating a cavity in between, in which light can bounce repeatedly summoning more and more coherent photons, until some of them pass through the non-perfect mirror to the outside (laser beam) as shown in Fig: 2-3.

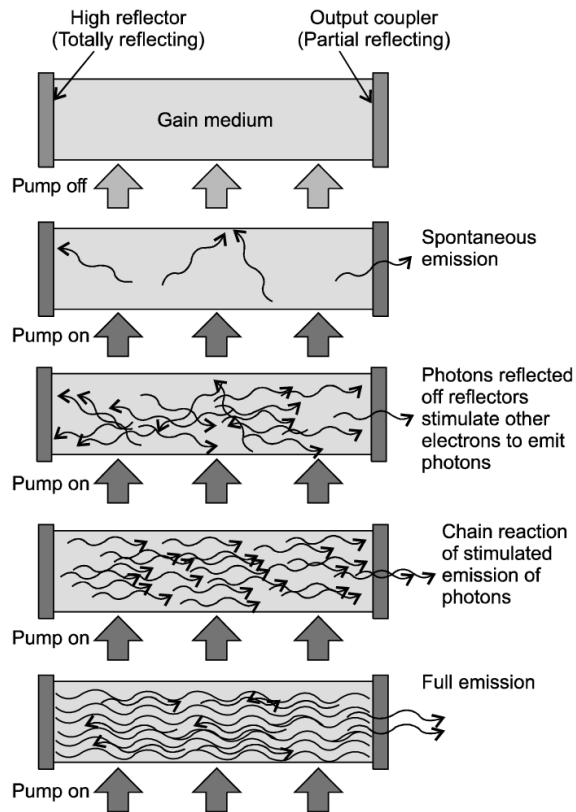


Figure 2-3: Schematic of laser emission. [Ki,11]

One of the advantages of this technique is that only those photons that travel perpendicularly to the mirrors are confined into the cavity, while the rest of them are able to exit the cavity without much interaction. Therefore, the efficiency losses from undesired stimulated emission are reduced.

A particular set of laser glasses are the up-converter laser glasses. In most cases, the pumping light has a lower wavelength (higher energy) than the emitted light, but in the case of up-converters, the pumping light has lower energy. The stimulation of the atoms to a high enough level requires a multiphoton process which is usually obtained by using two different RE ions, one with the emission desired level, and a pumping one, whose main purpose is to absorb pumping light, and to deliver the high energy electrons to the emitting ions.

This study is centered in the Er-Yb codoping for upconversion. Both rare earths are presented as their trivalent cations,  $\text{Er}^{3+}$  &  $\text{Yb}^{3+}$ . This codoping is interesting as it allows for near infrared (NIR) to visible light frequency up conversion as shown below.

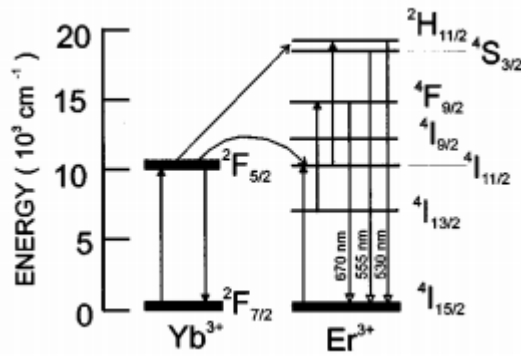


Figure 2-4: Simplified energy level diagram of Er<sup>3+</sup>/Yb<sup>3+</sup> ions. Upwards arrows indicate excitation photons and downwards arrows stand for emission photons [OI,98].

The typical upconversion fluorescence spectrum of a Er<sup>3+</sup>:Yb<sup>3+</sup> codoped glass under  $\approx 1\mu\text{m}$  irradiation show peaks centered around 530, 555, 670, 830, and 925 nm, corresponding to the transition from  $^2\text{H}_{11/2}$ ,  $^4\text{S}_{3/2}$ ,  $^4\text{F}_{9/2}$ ,  $^4\text{I}_{9/2}$ , and  $^4\text{I}_{11/2}$  excited levels to the  $^4\text{I}_{15/2}$  ground state, respectively [OI,98]. Previous studies show that codoping with Yb, increases Er upconversion efficiency up to 25 times in Ga:La:S chalcogenide glass [OI,98].

## 2.1.2 Biomaterials

Biomaterials have been defined as “any substance or combination of substances, other than drugs, synthetic or natural in origin, which can be used for any period of time. They can augment or replace partially or totally any tissue, organ or function of the body. They are used to maintain or improve the quality of life of the individual” by the American Institute of Health [Be,13]. In other words, a biomaterial is anything that after having been implanted in a body, it substitutes or even helps in the recovering of any tissue, organ or body function.

Materials for biological applications have since been classified depending on the reaction of the surrounding tissue, and the interface between the tissue and the material over time. This classification is as follows:

- **Non-biocompatible materials** which are composed of **cytotoxic materials**. This group encompasses materials that kill their surrounding tissue. Examples of substances in this group are Pb or As. There are also **carcinogenic materials**, which don't kill the surrounding tissue but promote the growth of tumors, substances such as Cd or Benzene, belong to this group.
- **Biocompatible materials** which are composed of different biocompatible materials which are schemed in Fig: 2-5

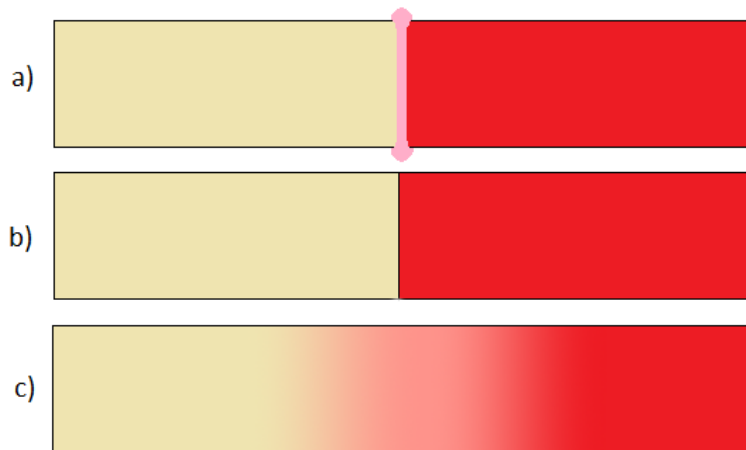


Figure 2-5: Scheme of different biocompatibility degrees: biotolerance (a), bioinertness (b) bioactivity (c)

**Biotolerant materials** promote the development of a conjunctive tissue layer between the material and the rest of the body. This “capsule” remains after the recovery from the wounds coming from the implantation, acting as a barrier isolating the foreign material. Most of the materials historically used for biomedical applications, such as stainless steel, are part of this group.

**Bioinert materials** don't show any kind of reaction from the body after the initial recovery, or the response is too little to be significant. Titanium is a bioinert material.

**Bioactive materials** promote a desired controlled response from the surrounding tissue. They usually show properties such as biosorption and osseointegration. The materials in this group can further be classified into two subclasses: class A promotes bone ingrowth where the bone was not present, while class B promotes interface bone-implant.

The use of biomaterials goes back to ancient Egypt and Rome, and were based on using metals such as gold or materials from organic sources such as wood, ivory or animal sinew [NI,20]. In the 20<sup>th</sup> century, polymethyl methacrylate (PMMA) was introduced to the list as the first polymer and the first synthetic biomaterial. The field has developed significantly since. Initially, metals such as Titanium seemed to be the best material for the application, due to its outstanding mechanical properties. However, uncoated metals, even when non-toxic, exhibit a bioinert or biotolerant behavior, not allowing for deep continuous integration with the surrounding tissue (biointegration) [Be,13]. Therefore, ceramics have emerged as promising candidates as they allow cell ingrowth [Be,13].

### 2.1.3 Bioactive glasses

Bioactive glasses are osteoconductive and osteoinductive materials that have been defined as materials that undergo specific surface reactions leading to the formation of a hydroxyapatite (HA) like layer after implantation in the body. HA is a phosphate mineral with specific stoichiometry  $(Ca_{10}(PO_4)_6(OH)_2)$ . Nevertheless, it can generally include any apatite calcium phosphate with major structural and compositional characteristics of HA,

usually deviating from stoichiometric composition [Hu,06]. The HA-like layer forms a bond to both soft and hard tissues simultaneously [Ko,06]. The capability of forming this HA-like layer after immersion in simulated body fluid (SBF) in vitro is often taken as an indication of the bioactivity response of a material [Ko,90]. Additionally, this in vitro bioactivity has been suggested as an indication of the material's potential bioactivity in vivo [He,71] [He,91] [Ra,11].

In an ideal situation the decomposition rate of the glass equals the regeneration rate of the surrounding tissue, providing enough support while not permanently remaining in the body [Jo,15]. A bioactive glass, when implanted is expected to completely dissolve while promoting bone growth, but this statement doesn't always hold true, as there has been evidence of glass remnants years after implantation [Li,10].

There are several types of bioactive glasses, from conventional silicate glasses, such as Bioglass, to newer kinds such as phosphate and borate-based glasses. Recently the interest on borosilicate glasses has increased due to their exceptional behavior in the treatment of chronic wounds, such as ulcers [Fu,10]. On the other hand, phosphate glasses benefit for fast solubility [Ro,18].

## 2.2 Bioactive scaffolds

Porous scaffolds in tissue engineering play an important role in controlling cell function and guiding new organ formation [Ch,02]. A scaffold is in essence a 3D temporary structure to which isolated and expanded cells adhere in all three dimensions (Fig: 2-6). A structure where the cell can proliferate, and secrete their own extracellular matrices, replacing the biodegrading scaffold [Ch,02].

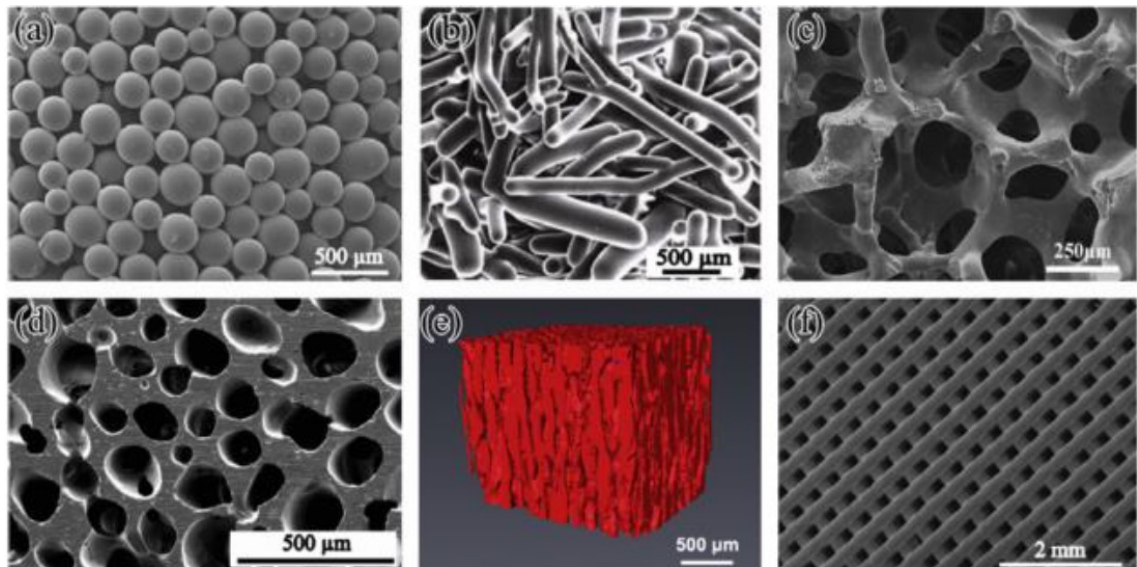


Figure 2-6: Microstructures of bioactive glass scaffolds created by a variety of processing methods [Ra,11]

Significant challenges to this approach include the design and fabrication of the scaffolds.

### 2.2.1 Materials used for the fabrication of scaffolds

Several different materials have been tested for the fabrication of solid scaffolds and they can be grouped into three different categories: Linear aliphatic polyesters, natural macromolecules and inorganic materials.

**Linear aliphatic polyesters:** Polylactic acid (PLA), polyglycolic acid (PGA) and their copolymers (PLGA), are the most used family of aliphatic polyesters in tissue engineering. These polymers degrade in the body by hydrolysis of their ester bonds. PGA has a very fast degradation rate (loss of mechanical stability between two and four weeks), while the more hydrophobic PLA degrades slower (mechanical integrity lost in several months or even years) [Ma,04]. PLGA are among the few approved by the American Food and Drug Administration (FDA) for certain human clinical applications. Other used aliphatic polyesters are poly  $\epsilon$ -caprolactone (PCL) and poly hydroxy butyrate (PHB) whose degradation rates are even slower than PLA making them less interesting for tissue engineering applications, but more attractive for long term implants and controlled release applications [Ma,04].

**Natural macromolecules**, such as proteins and polysaccharides, have also been used for tissue engineering. Collagen is a fibrous protein that is a major component in the extracellular matrix. This protein has been widely used for soft tissue repair and copolymerized into collagen-glycosaminoglycan (CGAG) to fabricate scaffolds for tissue engineering. Denaturalized collagen (Gelatin) has also been processed into porous materials for tissue repair. In the other hand, collagen presents some issues such as potential pathogen transmission, immune reactions, handling, mechanical properties and less controlled biodegradability. Silk is another widely used natural fibrous protein in the field of tissue engineering. Silkworm silk shows in vivo degradation from enzymatic mechanism, but the rate is very slow. There are also some concerns over its cytotoxicity. The last group of natural materials widely used are polysaccharides. For example, alginate, chitosan, and hyaluronate have been used as porous solid-state tissue engineering scaffolds. Apart from the relatively pure natural materials, processed extracellular matrix (denaturalized) materials with several natural macromolecules are also used as scaffolds for tissue engineering or repair, such as internal intestinal submucosa, porcine heart valves, or human dermis. Again, there are big concerns about pathogen transmission and immune reactions.

**Inorganic materials** have also been studied for bone and other mineralized tissue engineering research. Both natural and synthetic inorganic materials have been researched in the recent years. Natural inorganic scaffolds such as coral, mineralized silk proteins, and antlers possess suitable biocompatibility and osteoconductive properties because they are structurally similar to the mineralized tissues in the body. In the other end of the spectrum, are the synthetic inorganic materials, these materials are from the ceramic family of materials. The most studied among these materials are synthetic hydroxyap-

atite (HA), Nano HA, Bioglass, Beta Tricalcium Phosphate ( $\beta$ TCP), and Calcium Phosphate (CaP) [Ta,12]. The advantages from this type of materials are the lower concern about pathogen transmission and immune reactions. However, a less specialized structure than that of organic materials is their main drawback. Therefore, intense research is being conducted to simulate the structure of organic materials with inorganic ones.

## 2.2.2 Requirement for glass scaffolds and their fabrication process

Bioactive glasses come in several different forms and sizes, as shown in Fig: 2-7, and the specifics of their behavior is dependent on the specific geometry [Yl,00] [Hu,12] [Zh,12] [De,12] [Fa,12].

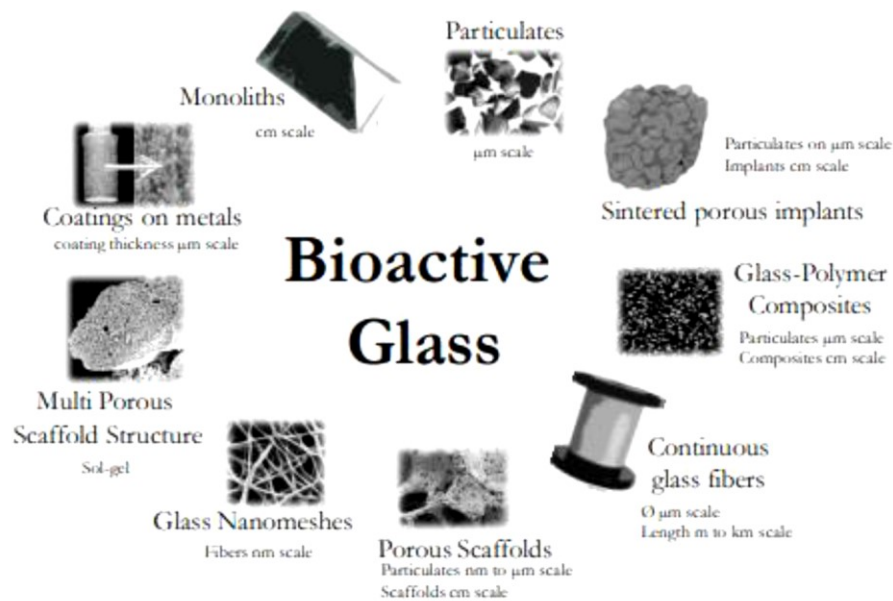


Figure 2-7 Different bioactive glasses available [Fa,12]

Different geometries show different pore shape, size and connection as well as glass' specific surface area, changing the characteristics of the contact between the glass and the body. For example, higher surface area enhances reactivity and dissolution rate, while the porosity requires certain characteristics of minimum pore size and open connectivity to allow tissue ingrowth and neovascularization [Li,07]

3D Scaffolds have been used to grow cell [Su,04]. To be promising, scaffolds need to possess the following properties

- 1) Have high porosity (>50%), and proper pore size (~100µm).
- 2) High surface area.
- 3) Mechanical integrity to maintain the predesign tissue structure.
- 4) Biocompatibility and bioactivity
- 5) Biodegradability and a proper degradation rate matching the formation of new tissue

Different approaches to fabricate bioactive glass has been developed [Fu,11], such as electrospinning of a sol-gel to create nanofibers [Hu,12] [De,12], sintering of microspheres [Yl,00] or glass powder [Go,01] to achieve highly porous structures, sol-gel infiltration of polymer foam [Li,07], freeze casting [De,06] or solid free forming [Ho,05] [Fu,11 (2)].

### 2.2.3 Borosilicate scaffold

Borate and borosilicate bioactive glasses have been prepared [Ya,07] [Fu,10]. When compared to silicate glass, borate bioactive glass was found to degrade faster and completely convert to HA because of its low chemical durability [Hu,06]. As such, the degradation rate of the glass can be tailored to the desired value by adjusting the  $\text{SiO}_2 / \text{B}_2\text{O}_3$  ratio, allowing the production of a bioactive glass with a degradation rate matching bone regeneration rate [Ra,11].

An interesting family of borosilicate glasses is the glass system corresponding to the S53P4 bioactive glass system (commercially available as BonAlive®) . These glasses adhere to the following composition:  $(53.85 - x) \text{SiO}_2 - x\text{B}_2\text{O}_3 - 22.66 \text{Na}_2\text{O} - 1.72\text{P}_2\text{O}_5 - 21.77 \text{CaO}$  with  $x$  varying from 0 to 53.85 in mol%. These glasses are usually labelled by the  $\text{B}_2\text{O}_3 / (\text{SiO}_2 + \text{B}_2\text{O}_3)$  ratio (B0 (S53P4), B25, B50, B75 and B100). These glasses show interesting properties, such as moderate glass transition temperature ( $500 < T_g < 550^\circ\text{C}$ ) and  $\Delta T > 100^\circ\text{C}$ , indicating that these glasses are stable against crystallization [Ma,12] [Oj,16] [Fa,17] [Pr,18]

Among the glass family, the 50% substitution of  $\text{SiO}_2$  by  $\text{B}_2\text{O}_3$  (B50) was found to exhibit the most interesting balance of properties among the family [Oj,16] [Fa,17] [Oj,18], and is the focus material of this work. [Oj,18]. The sintering analysis of the borosilicate glass was performed by differential thermal analysis, and surface crystallization was found to be the main crystallization mechanism. The glass was sintered into porous scaffolds and the effect of the particle size and sintering temperature was analyzed. Amorphous scaffolds were successfully processed with porosity ranging from 10 to 60% and with compressive strength from 1 to 35MPa. The scaffolds retained their capabilities to rapidly create an HA layer with a faster rate than the FDA approved S53P4 bioactive glass [Oj,16] [Fa,17]. The cell behavior of the B50 scaffolds was also evaluated. Despite reducing hASC proliferation and inhibiting cell pro, the B50 glass stimulates osteogenic commitment and upregulate endothelial markers, thus supporting their further evaluation for regenerative medicine [Oj,18].

B50 is reported with the following properties [Fa,17] [Oj,16] [Oj,18]:

- $T_g = (510 \pm 2)^\circ\text{C}$ ,  $T_x = (675 \pm 2)^\circ\text{C}$ ,  $T_p = (724 \pm 2)^\circ\text{C}$  &  $\Delta T (T_x - T_g) = (165 \pm 4)^\circ\text{C}$ .
- $E_a = (250 \pm 30) \text{kJ/mol}$ , & crystallization speeds of  $(95 \pm 12)$ ,  $(72 \pm 11)$  &  $(49 \pm 2) \mu\text{m/h}$  at  $T_p - 20, 40$  &  $60^\circ\text{C}$  respectively.
- Compressive strength of  $\approx 2.5 \text{MPa}$  for scaffolds with 50% porosity.
- Higher dissolution rate than pure silica scaffolds.
- Comparable osteogenic properties to unmodified S53P4

## 2.3 Drug delivery systems

Drug delivery systems (DDS) have been designed to improve the pharmacological and therapeutic properties of drugs administered parenterally [Al,04]. Their main purpose is to control the delivery of a drug either in space, time or in both at the same time.

In conventional drug delivery, either by oral or intravenous route, the drug spreads along the whole body, even if the infected area is highly localized resulting in higher drug dosage as well as in potential side effects.

The use of spatially localized drug release allows only the medication to the afflicted zone. This opens the possibilities to use cytotoxic drug which also destroys the surrounding tissue when the delivery can be properly controlled. Such localized drug delivery systems offer a very promising possibility to treat cancerogenic tumors.[Si,12]. Additionally, the drug concentration profile over time spikes after every dose intake when using conventional drug administration, the profile decreasing afterwards. Therefore, this localized drug release process produces an oscillating value of the concentration that can reach both toxicity concentrations as well as ineffective concentration ranges as depicted in Fig: 2-8

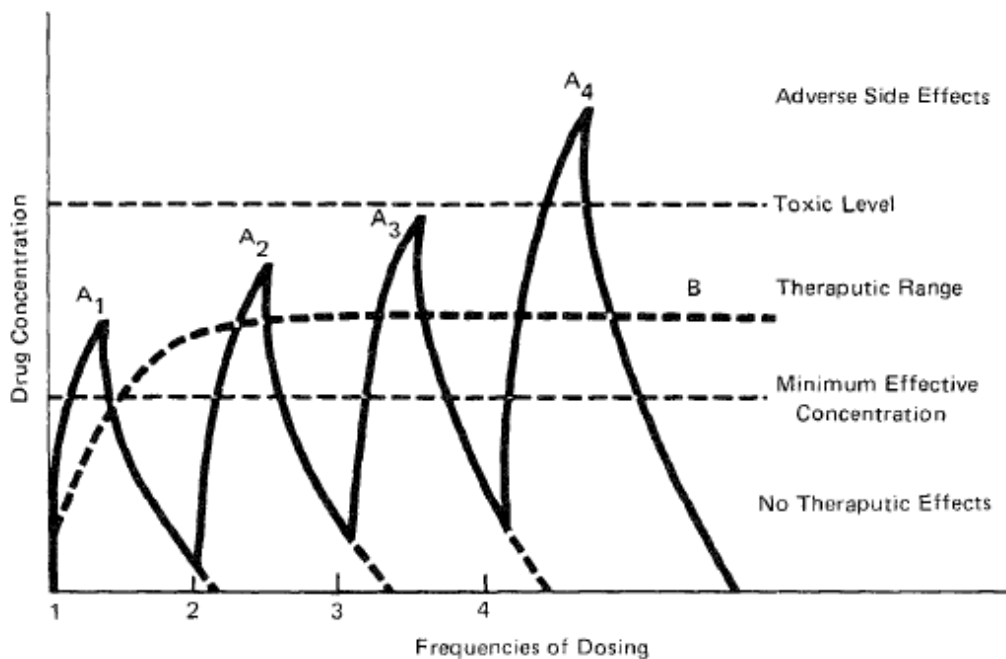


Figure 2-8: Hypothetical drug concentration profiles in the systemic circulation resulting from the consecutive administration of multiple doses of an immediate-release drug delivery system (A), A<sub>2</sub>, ••) compared to the ideal drug concentration profile (B) required for treatment. [Yi,91]

In Fig: 2-8 we can observe the advantages of the DDSs, where the concentration profile can steadily remain in the ideal concentration range, allowing the drug to act all the time, while not giving adverse side effects.

### 2.3.1 Localized drug delivery systems

The DDSs can be classified based on their technical sophistication as shown in Fig: 2-9

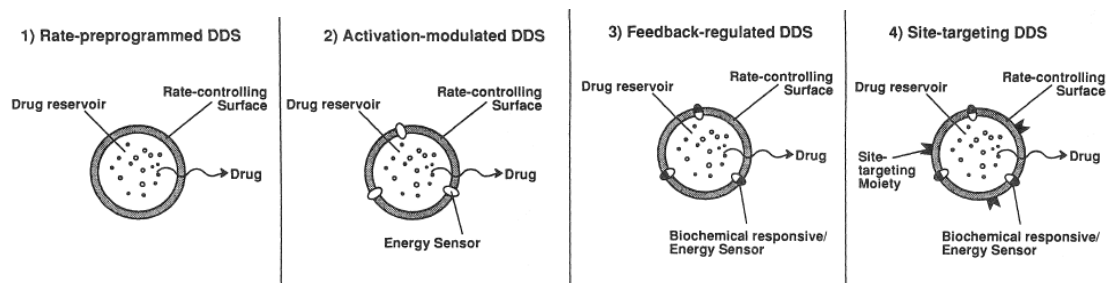


Figure 2-9: Classes of DDSs [Yi,91]

**Rate-preprogrammed drug delivery systems** encompasses those DDSs in which the delivery systems have been preprogrammed at specific rate profiles. This is accomplished by system design, which controls the molecular diffusion of drug molecules in, and/or across the barrier medium within or surrounding the DDS. In this kind of system, Fick's diffusion laws are usually followed. Release rate and profile are obtained by choosing the optimal capsule materials and geometry [Yi,91].

**Activation-modulated drug delivery systems** encompasses those DDSs in which the release of drug molecules from the DDS is activated by some physical, chemical, or biochemical processes and/or facilitated by the energy supplied externally. The regulation of the drug release is controlled by the regulation of the applied process, or energy input [Yi,91].

**Feedback-regulated drug delivery systems** encompasses those DDSs activated by a triggering agent, such as a biochemical substance and regulated by its concentration via some feedback mechanisms. The drug delivery rate for this system is controlled by the concentration of the triggering agent [Yi,91].

**Site-targeting drug delivery systems** encompasses those DDSs that can attach themselves to specific target molecules. These target molecules are only present in certain locations, either by being organ specific, or by depending on the disease. These systems usually take use of the antigen antibody combination in order to lock their targets [Yi,91].

Although the use of DDSs shows promising properties, several challenges have to be solved before the use of any new DDS. These problems are mainly the design of a compatible drug reservoir compartment to both the drug and the body, the attachment of a rate-controlling element to the reservoir, or the implementation of the reservoir as the rate-controlling element itself, the control of the energy source, and the distribution of the DDS in the organism [Yi,91].

### 2.3.2 Proposed localized drug delivery system

This project focuses on the development of light activation modulated DDS. Our DDS is a scaffold made of a biophotonic glass loaded with a photocleavable molecule which is cleaved using green light.

In order to be able to obtain the activation signal to the DDS, the signal has two possibilities, either to come from the outside of the body or it has to be produced around the DDS. As shown in Fig: 2-10, green light cannot be used as the skin absorbs this wavelength.

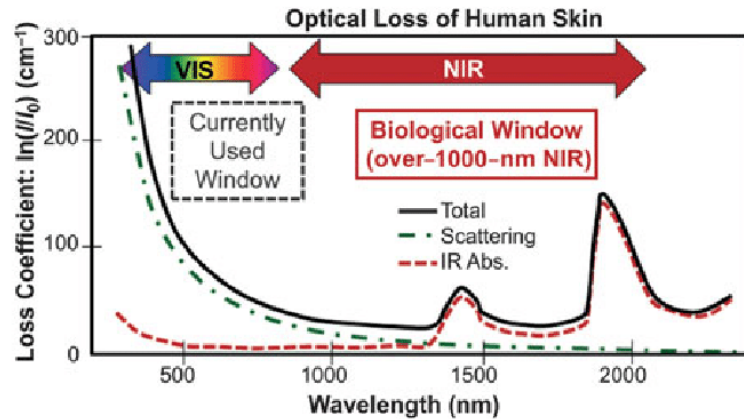


Figure 2-10: Absorption spectrum of human skin [He,14].

NIR is the most appropriate wavelength to use to activate the DDS through the skin. 980nm excitation was chosen for this study due to low absorption of 980nm radiation by the skin (Fig: 2-10). Therefore, our proposed DDS requires a two-step activation: as a first step, the proper modulation of the activation 980nm excitation passes through the skin into the implant location which is then converted into visible light to activate the photocleavable molecule as illustrated in Fig: 2-11.

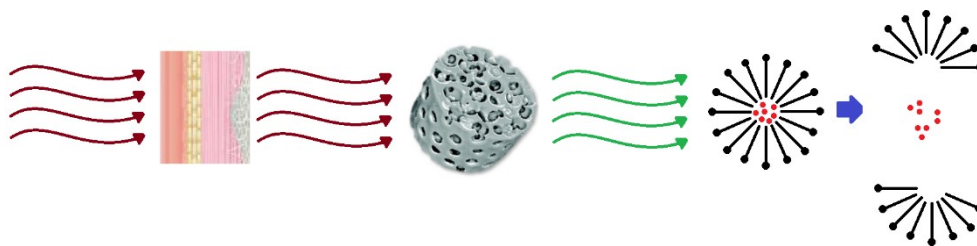


Figure 2-11: Modified schematic of the proposed DDS from [Zh,17]

The production of visible light can be approached in several different ways such as permanent luminescence, electroluminescence, thermoluminescence and photoluminescence. In order to properly control the drug dose, the permanent luminescence approach cannot be taken. Thermoluminescence would require large changes in the temperature in order to obtain signal. However, this temperature change would damage the surrounding tissue, discarding thermoluminescence as an option. From the two remaining

choices, this work focuses on photoluminescence for its lower invasiveness. Green emission will be obtained from the upconversion process.

Therefore, the biophotonic glass will be B50 glass which will be prepared with  $\text{Er}^{3+}$  and  $\text{Yb}^{3+}$  ions in order to exhibit green upconversion under 980nm excitation. Different scaffolds were prepared in this study in order to fabricate a scaffold with strong green upconversion.

## 3. MATERIALS AND METHODS

### 3.1 Material's preparation

In this study, active scaffolds were prepared by adding  $\text{Er}^{3+}$  and  $\text{Yb}^{3+}$  ions in the B50 glass and also by adding  $\text{NaYF}_4: \text{Yb}^{3+}, \text{Er}^{3+}$  nanocrystals in the B50 glass powder prior to sintering in order to prepare scaffolds with strong green upconversion under 980nm pumping to photocleave the molecules.

#### 3.1.1 Glass preparation

The glass of investigation was 26.93( $\text{SiO}_2$ )-26.93( $\text{B}_2\text{O}_3$ )-22.66( $\text{Na}_2\text{O}$ )-1.72( $\text{P}_2\text{O}_5$ )-21.77( $\text{CaO}$ ) (in mol%) and it is labeled B50. It was prepared using  $\text{SiO}_2$  (Umicore, 99.99%),  $\text{Na}_2\text{CO}_3$  (Honeywell, >99.5%),  $\text{H}_3\text{BO}_3$  (Sigma Aldrich, >99.5%),  $\text{CaCO}_3$  (Alfa Aesar, 99%), and  $\text{CaHPO}_4 \cdot 2\text{H}_2\text{O}$  (Sigma Aldrich, 98%). The glasses were made using the following heat cycle: First the mixed batch was placed inside the furnace at room temperature and heated up to 650°C at a rate of 10°C/min, for 10 min and then to 850°C for 10 min for the decomposition the precursors. Finally, it was melted at 1250°C for 10min. After quenching, the glass was annealed at 400°C for 6h to remove residual stresses from the quench.

Nanocrystals with the composition  $\text{NaYF}_4: \text{Er}^{3+}, \text{Yb}^{3+}$  were mixed prior to the sintering with the B50 glass. The synthesis and properties of the nanocrystals can be found in [Ha,11] [Pa,16] [Hy,16]

The  $\text{Yb}^{3+}, \text{Er}^{3+}$  co-doped glasses were produced by adding  $\text{Er}_2\text{O}_3$  and  $\text{Yb}_2\text{O}_3$  in the B50 glass. The composition of the glass was  $(1-x-y) 26.93(\text{SiO}_2)-26.93(\text{B}_2\text{O}_3)-22.66(\text{Na}_2\text{O})-1.72(\text{P}_2\text{O}_5)-21.77(\text{CaO}) - x\text{Er}_2\text{O}_3 - y\text{Yb}_2\text{O}_3$  with x varying between 0 and 0.03 and y between 0 and 0.08. The raw materials for the rare-earth ions were  $\text{Er}_2\text{O}_3$  (Sigma Aldrich, >99%), and  $\text{Yb}_2\text{O}_3$  (Sigma Aldrich, >99.9%). The melting procedure was the same than the one used for the melting of B50 glass.

#### 3.1.2 Scaffolds sintering

Scaffolds were prepared using the porogen burn-off technique. After annealing, the glasses were crushed using planetary ball milling technique. This technique is a grinding method that uses balls as the grinding medium, as they get moved violently by external forces (rotatory) mechanically crushing the sample into fine powder. The balls motion as well as the powder size and shape distribution depend on operational conditions. Fig: 3-1 shows the milling mechanism in a planetary ball mill [Mio,04]

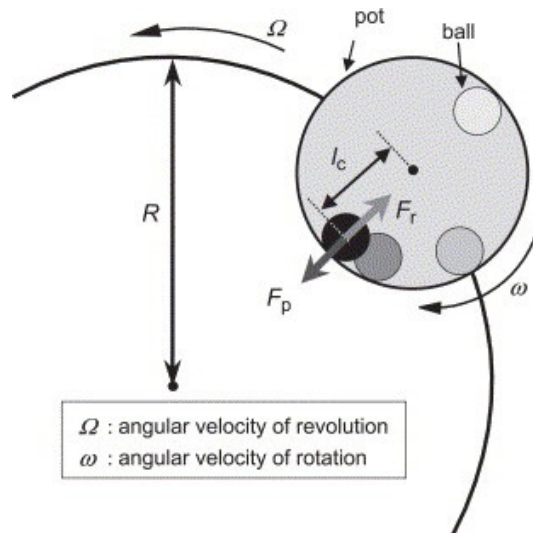


Figure 3-1: Ball milling mechanism. [Mio,04]

The system used in this study was FRITSCH PULVERISETTE 7 premium line Planetary Ball Mill under the following conditions:

- ZrO<sub>2</sub> balls and bowls.
- 10 balls per bowl.
- 10mm diameter balls.
- 850rpm.

Runs consisted in the following cycle: 2-minute milling + 1 minute cool down + 2 minute milling.

The Grinded powder was sorted by size using sieves. To properly control the particle size distribution, two different sizes of the sieve were used, one with the desired maximum particle size (38 $\mu$ m) and one intermediate size (150 $\mu$ m) to separate big fragments from the rest of the glass powder. The system used for the sieving was Retsch analytical sieve shaker AS200 Basic.

The crushed powder was mixed with the porogen, NH<sub>4</sub>HCO<sub>3</sub> (Sigma Aldrich, >99.5%) at a 0.3/0.7 (glass/porogen) ratio. This mixture was shaped into a cylindrical shape with a diameter of 15mm. The powder was pressed under 20GPa. The pellets were sintered at 300°C using a rate of 1°C/min to allow the decomposition and evaporation of the porogen. After reaching 300°C, the heating rate was increased to 5°C/min to reach the sintering temperature. The sintering was for one hour. After sintering, the scaffolds were stored in a desiccator. The sintering temperature depended on the glass composition: 567°C was used to sinter the Er<sup>3+</sup>, Yb<sup>3+</sup> codoped scaffolds and 550°C to sinter the particles containing scaffolds and the undoped scaffolds.

### 3.1.3 Photocleavable molecules

In this study, a photoswitchable molecule was tested as a proof of concept for photocleavable molecular structures. The chosen molecule was Phthalimide-Azo-Iperoxo (PAI) (Fig: 3-2).

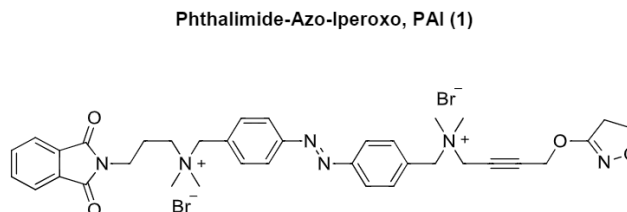


Figure 3-2: PAI photoswitchable molecule [Ri,19].

This molecule shows a trans-cis isomerism and exhibits photoswitching when exposed to the proper radiation. When the molecule is exposed to 365nm radiation, the molecule is promoted to change into the meta stable cis-Pai isomer, while irradiation at 460nm promoted the reversion into the more stable trans-Pai isomer [Ri,19] as seen in the absorption spectra of trans and cis isomers displayed in Fig:3-3.

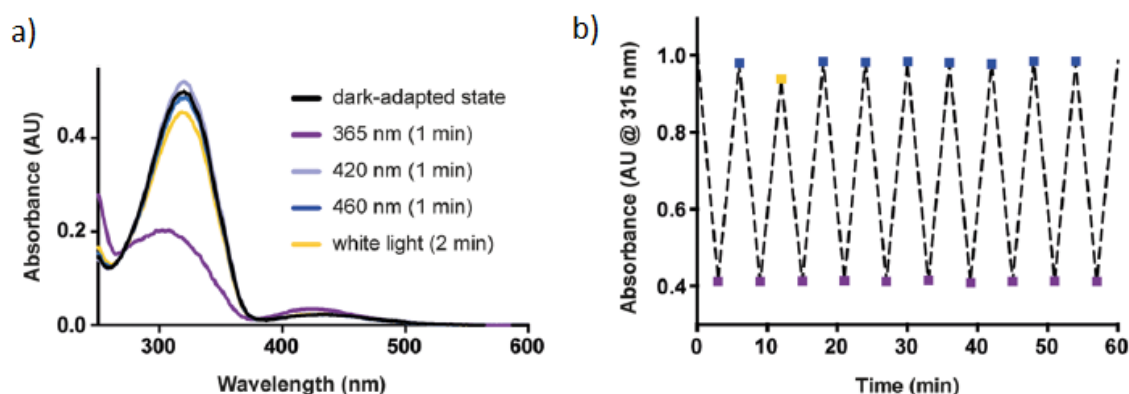


Figure 3-3: Absorption spectra of PAI after different irradiation (a) and absorbance over several irradiation cycles (b) [Ri, 19]

Fig: 3-3 b shows that photoswitching can be repeated for several cycles without noticeable photofatigue. [Ri,19]

The photocleavable molecules were provided by Dr. Rossella Castagna from Institute for Bioengineering of Catalonia (Spain).

## 3.2 Material's properties

### 3.2.1 Physical properties

The density was measured using Archimedes' principle. The immersion liquid ethanol was used, and the measurements were performed at room temperature. The mass of the sample was measured in air and then when immersed in Ethanol. The density of the glass was then calculated using the Eq.1:

$$\rho = \rho_{ethanol} \cdot \frac{w_{air}}{(w_{air} - w_{ethanol})} \quad [1]$$

Where  $\rho$  is the sample density,  $\rho_{ethanol}$  is the density of ethanol at measured temperature,  $w_{air}$  is the weight of the sample in air and  $w_{ethanol}$  is the weight of the sample in ethanol.

The equipment utilized was OHAUS Adventurer Analytical scale and the corresponding kit to calibrate the equipment before measuring the samples. The density is measured with an accuracy of  $\pm 0.02 \text{g/cm}^3$ .

### 3.2.2 Thermal properties

The thermal properties were analyzed by differential scanning calorimetry (DSC) using 449 F1 Jupiter (Netzsch-Gerätebau GmbH, Selb, Germany) equipment. Samples were measured by placing 30mg sample (powder form) in a Pt pan. Their heat absorption was compared to that of a reference Pt pan of similar mass while keeping sample and reference at the same temperature and while increasing the temperature at a constant rate of  $10^\circ\text{C/min}$ .

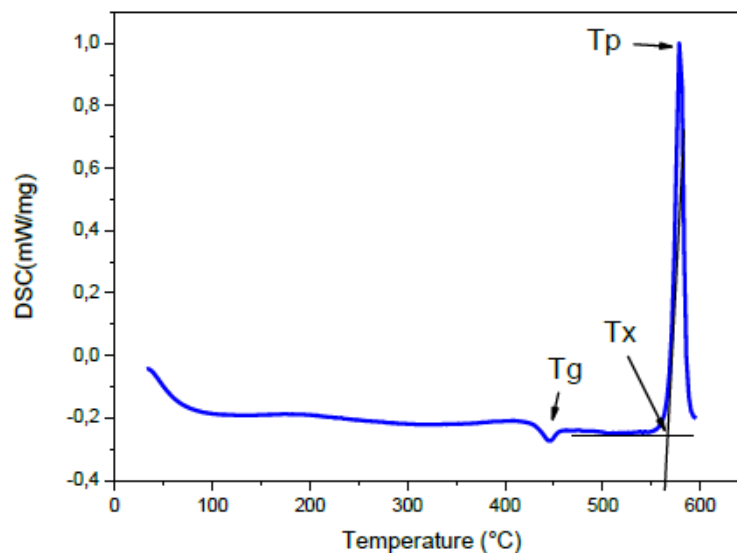


Figure 3-4: Thermogram of a glass.[Ro,18]

From the DSC curve (Fig: 3-4), several important information can be obtained such as the glass transition temperature ( $T_g$ ), the crystallization temperatures (temperature onset

of the crystallization peak ( $T_x$ ), and crystallization peak temperature ( $T_p$ ).  $T_g$  was defined as the inflection point in the thermogram and  $T_p$  at the maximum of the crystallization peak. The precision of these temperatures is given at 3°C. Another important parameter is  $\Delta T$ , which is defined as the difference between  $T_x$  and  $T_g$  and is related to the thermal stability of the glass against crystallization. The resolution of this temperature window span is of 6 °C.

Other significant parameters can be obtained, such as specific heat by measuring the slope of the curve or phase transformation latent heat by measuring the areas under/below the phase transformation peaks.

### 3.2.3 Optical properties

The absorption spectra were measured using UV-3600 Plus UV-VIS-NIR Spectrophotometer Shimadzu. This device, the schematic of which can be found in Fig: 3- 5, produces polychromatic light from a lamp (or several different ones), and passes this light through a monochromator resulting in the selection in a narrow bandwidth of the source spectrum. The “monochromatic” light is divided by a beam splitter (50/50) and the two resulting beams are passed through both the sample and a reference. The transmitted light is then collected and measured by a detector.

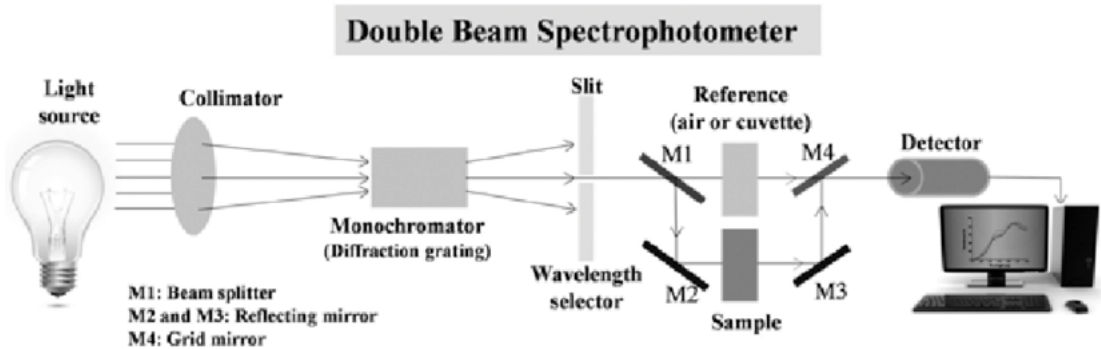


Figure 3-5: Schematic of a double beam spectrophotometer [Je,15]

The spectrometer sweeps through the required wavelength range adjusting the monochromator and the source lamps and calculates the absorbance at a specific wavelength by the comparing the intensity from the reference and the sample. This measurement allows the obtention of the absorbance spectrum of the material, which is helpful to calculate the absorption coefficient and cross-section, two parameters which are intrinsically related to the ions site in the glass, and ultimately to the glass photonic properties.

The Beer–Lambert Law (Eq.2.) relates the absorbance ( $A$ ) with the transmitted and incoming intensities ( $I_T$ ,  $I_0$ ) and the material’s thickness ( $t$ ) and absorption coefficient ( $\alpha$ ).

$$A = -\log_{10} \frac{I_T}{I_0} = \int \alpha t dt \quad [2]$$

The absorption cross-section ( $\sigma$ ) is related to the absorption coefficient and the number of ions per unit volume ( $N$ ) by Eq.3.:

$$\sigma = \frac{\alpha}{N} \quad [3]$$

### 3.2.4 Spectroscopic properties

The up-conversion emission spectra in the 350-800nm range were measured using a Jobin Yvon iHR320 spectrometer (Horiba Jobin Yvon SAS, Unterhaching, Germany) equipped with a Hamamatsu P4631-02 detector (Hamamatsu Photonics K.K., Hamamatsu, Japan) and a filter (Thorlabs FEL 1500, Thorlabs Inc., Newton, NJ, USA). Emission spectra were obtained at room temperature using an excitation monochromatic source at 976 nm, emitted by a single-mode fiber pigtailed laser diode (CM962UF76P-10R, Oclaro Inc., San Jose, CA, USA).

Emission is due to the relaxation of the electrons in the high energy states by radiative routes. The radiative relaxation routes emit photons that are collected by a detector. By placing a monochromator in the optical path between the sample and the detector, the emission at each specific wavelength can be detected, giving information of the emission spectrum of the sample.

Up conversion is based on multiphoton processes, where an already excited electron is further excited by a second photon before relaxing radiatively emitting a photon of higher energy than the absorbed ones as illustrated in Fig: 3-6, taken  $\text{Yb}^{3+}$ ,  $\text{Er}^{3+}$  codoping as an example.[Pa,16]

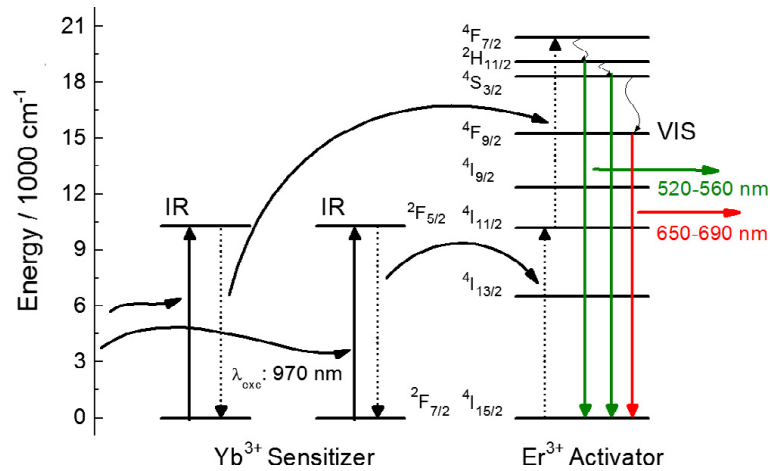


Figure 3-6: Schematic of upconversion, and proposed upconversion mechanism between  $\text{Yb}^{3+}$  and  $\text{Er}^{3+}$ . [Pa,16]

### 3.2.5 Mechanical properties

The mechanical properties of the scaffolds were tested in compression using Instron8800 equipment.

Standard compression testing was performed by compressing the scaffolds and recording the applied load and the displacement as a function of time. From this data, the engineering Stress-Strain ( $\sigma$ - $\epsilon$ ) curve was obtained, and from it, the compressive strength of the material can be determined.

The typical  $\sigma$ - $\epsilon$  curve of a highly porous linear elastic ceramic is shown in Fig: 3-7a:

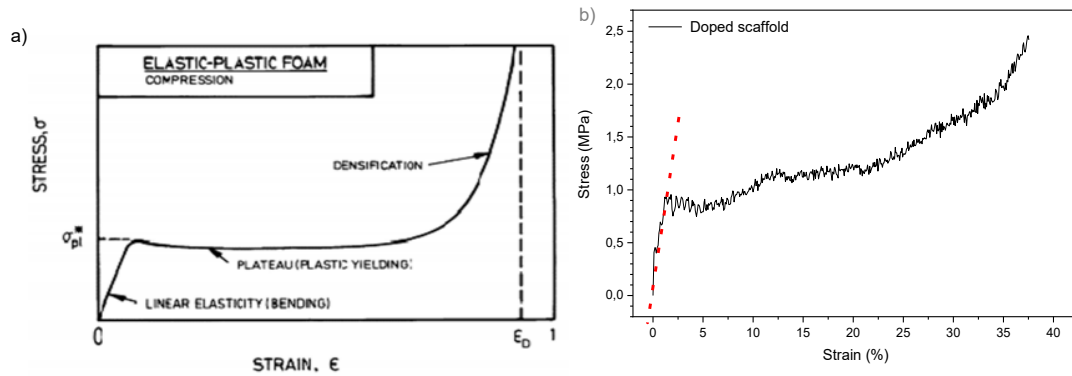


Figure 3-7:  $\sigma$ - $\epsilon$  curve of highly porous ceramic [Al, 12] (a) and of B50 + 1.5%NCs (b)

The typical  $\sigma$ - $\epsilon$  curve exhibits three different regions

- a first linear region, that showcase the elastic behavior of the material,
- a plateau region, that is related to the collapse of the porous structure
- a final non-linear increasing region that is related to the compression of the collapsed powder.

The only focus of the study of this project is the initial linear regime, where only elastic recoverable deformations take place, and the compressive strength given in this thesis is the stress value measured of the plateau strength.

The  $\sigma$ - $\epsilon$  curve of a scaffold prepared with the NaYF<sub>4</sub> nanocrystals, taken as an example is shown in Fig: 3-7b. The elastic regime can be attributed to deformations around 30%, measuring a compressive strength of  $(2.9 \pm 0.3)$  MPa, the minimum and maximum values are displayed in red and blue respectively. Moreover, the lack of plasticity of the glass can be seen from the lack of the plastic yielding plateau.

### 3.2.6 Porosity measurement

Porosity was estimated by measuring the volume of the cylindrical scaffold and its mass, obtained from the density using the Eq 4.

$$Porosity(\%) = 1 - \frac{\rho_{ap}}{\rho_{th}} = 1 - \frac{m/\pi D^2}{\rho_{th}} \quad [4]$$

### 3.2.7 In vitro testing

Glass scaffolds were immersed in simulated body fluid (SBF) following a mass to volume ratio of 10ml per 100mg for 24, 48, 72, 168, and 336 h at 37 °C in an incubating shaker (INFORS Multitron II). Three parallel samples were taken for each composition and time point. In the incubator, the orbital speed of 100 RPM was chosen to provide laminar flow mixing of the solution without altering the dissolution process by particle movement.

The change in the pH over time for the buffering solution was recorded for each immersion time and the average and standard deviation of the triplet was calculated. The pH was then compared to that of a blank sample which contains only the buffer. The equipment used was Mettler Toledo SevenMulti MP 225 pH-meter, and it shows a resolution of  $\pm 0.02$ . After testing, the scaffolds were washed by acetone and dried for their weighing.

### 3.2.8 X-ray diffraction analysis

XRD is a technique that gives information about the crystalline structure of a material by irradiating the sample with x-rays. XRD can be used to determine if a material is either amorphous or crystalline.

This technique is based on Bragg's diffraction law (Eq.5), and is sketched in Fig: 3-8:

$$2 * d * \sin(\theta) = n * \lambda \quad [5]$$

Where d is the inter planar distance,  $\theta$  is the incidence angle, n is any positive integer and  $\lambda$  is the wavelength of the x-ray.

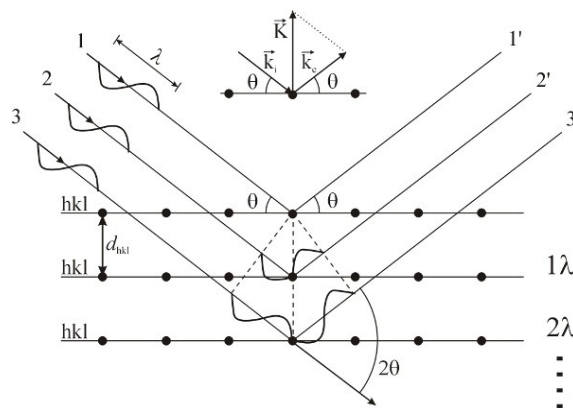


Figure 3-8: Sketch of XRD working principle [Ph,13]

The principle dictates that diffracted light interferes constructively only when the above expression is fulfilled, implying that the effective distance between crystalline planes to be travelled by the photons is equal to a multiple of the half wavelength [Wi,06].

The spectrum of any material is characteristic and most known crystalline materials have already been identified and tabulated. [Ch,01]. This allows the proper identification of any crystalline phase in the sample.

The measurements were carried out using Panalytical EMPYREAN multipurpose X-Ray Diffractometer equipment with Fe filtered Co- $k_{\alpha}$  radiation and a  $\theta$ - $2\theta$  configuration. Following the schematics shown in Fig: 3-9.

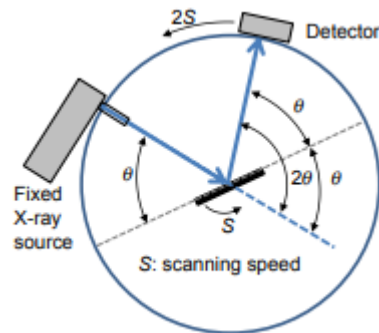


Figure 3-9: XRD set up in a  $\theta$ - $2\theta$  configuration (fixed x-ray source) [Ep,16].

X-rays are generated in the X-ray tube by impinging high energy electrons and emitting at the characteristic wavelength of the source material. The produced X-rays are filtered from unwanted lines and focused on the sample's surface. The diffracted X-rays are collected by the detector. The X-ray tube is fixed in position while the sample stage and the detector rotate in a  $\theta$ - $2\theta$  configuration to sweep most geometrical configurations.

### 3.2.9 Scanning electron microscope

Scanning electron microscope (SEM) is a powerful microscopy technique that uses electrons to obtain resolutions down to the nanometer scale.

The operating principle of SEM is to generate and accelerate electrons to high energies by a potential difference and focusing them into the sample. The electrons interact with the sample emitting different signals such as back scattered electrons (BSEs), secondary electrons (SEs) and X-rays. The interaction is confined to a small volume at the impingement zone. The studied area is swept by the beam point by point recording the information as if a pixel image was taken. This allows for the reconstruction of the sample's surface while providing some compositional information.

In SEM, the main signals are BSEs and SEs, these two signals are not collected simultaneously, and image usually only use one of them.

- SEs provide better topological contrast and is desired for its higher resolution.
- BSEs are very sensitive to the atomic number of sample's atoms, providing high compositional resolution.

The schematic of a SEM can be observed in Fig: 3-10.

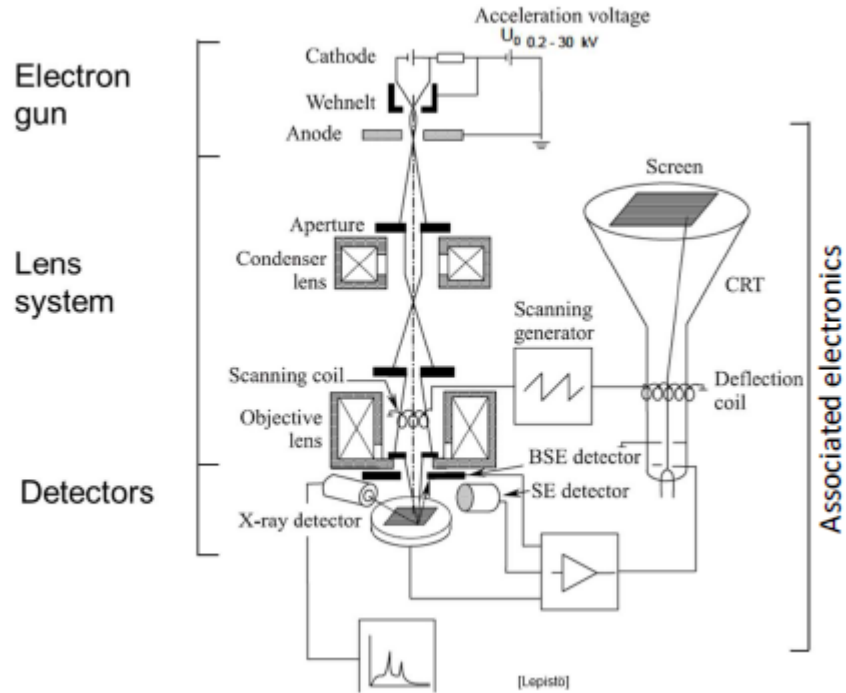


Figure 3-10: Schematics of a SEM [Go,12].

Currently most SEMs are equipped with an energy dispersion spectroscopy (EDS). This system uses the X-rays generated by the interaction between the electrons and the sample to analyze the elements present in the sample in a quantitative manner. When the electrons from the beam excite the atoms in the sample, they move their electrons to higher metastable energy levels, from which they relax, emitting X-rays of a characteristic energy. These energies depend only on the element and the excitation. The EDS system collects and analyzes the generated X-rays producing a spectrum. In this spectrum, the characteristic peaks from the elements present in the sample can be observed together with a background radiation produced by inelastic interactions between the electrons and the sample. It is possible to produce a quantitative evaluation of the elemental composition in different areas of the sample with a resolution about one mole percent [Go,12]. Fig: 3-11 shows a typical EDS spectrum.

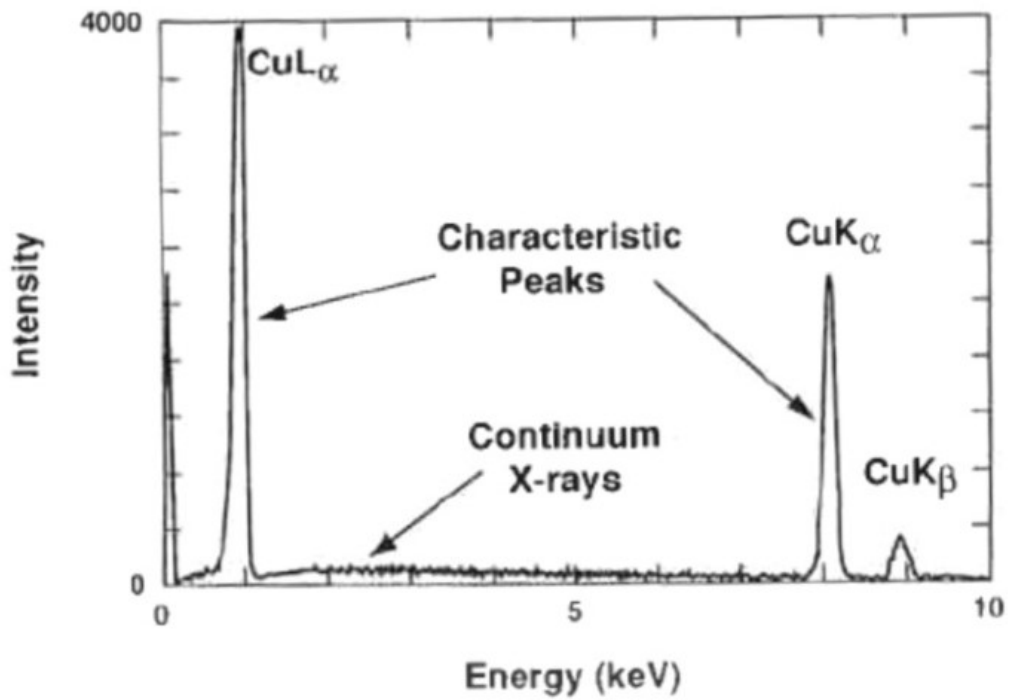


Figure 3-11: Typical EDS spectrum [Go,12]

EDS can be performed in line or mapping mode. These modes perform several individual point analyses (usually with lower capture times, reducing resolution) covering a whole line/area providing elemental information, and the variation through the investigated space.

The equipment used in this study was Carl Zeiss Crossbeam 540, with a Oxford Instruments X-MaxN 80.EDS detector.

## 4. RESULTS AND DISCUSSION

The main purpose of this study is to produce a NIR sensitive drug delivery system using photocleavable molecule. The objective of this study was the preparation of biphotonic scaffolds which not only are bioactive but also exhibit green emission under 980nm pumping to photocleave the photosensitive molecule after implantation in the body.

### 4.1 Preparation and characterization of scaffolds

In this study, the scaffolds were prepared using the burn off technique. At first, the glass is prepared using standard melting process, then crushed into powder and finally sintered. The glass of investigation is the borosilicate glass with the composition 26.93 SiO<sub>2</sub>-26.93 B<sub>2</sub>O<sub>3</sub>-22.66 Na<sub>2</sub>O-1.72 P<sub>2</sub>O<sub>5</sub>-21.77 CaO (in mole %) (Referred as B50). This glass was reported to be optimal for producing amorphous scaffolds while allowing hydroxy-carbonate apatite precipitation within the scaffold structure [Fa,17].

In order to obtain green emission from the scaffolds using 980 nm pumping, the B50 glass was prepared with Yb<sup>3+</sup> and Er<sup>3+</sup> ions. In this study, two series of scaffolds were fabricated:

- the Yb<sup>3+</sup> and Er<sup>3+</sup> ions were added in the glass batch prior to the melting. The scaffolds are labeled as Yb<sup>3+</sup>, Er<sup>3+</sup> doped scaffolds
- NaYF<sub>4</sub>:Yb<sup>3+</sup>, Er<sup>3+</sup> nanocrystals (NCs) with strong green upconversion under 980nm pumping were added in the glass crushed into powder prior to the sintering. These scaffolds are labeled as NCs scaffolds

#### 4.1.1 Yb<sup>3+</sup>, Er<sup>3+</sup> doped scaffolds

##### 4.1.1.1 Optimization of the Er<sub>2</sub>O<sub>3</sub> and Yb<sub>2</sub>O<sub>3</sub> content

The scaffolds were prepared from Yb<sup>3+</sup>, Er<sup>3+</sup> codoped borosilicate glasses. The concentration of Yb<sup>3+</sup> and Er<sup>3+</sup> had to be first optimized in order to prepare borosilicate scaffolds with strong green upconversion. Below is the picture of the glasses prepared with various Yb<sup>3+</sup> and Er<sup>3+</sup> content (Fig: 4-1).

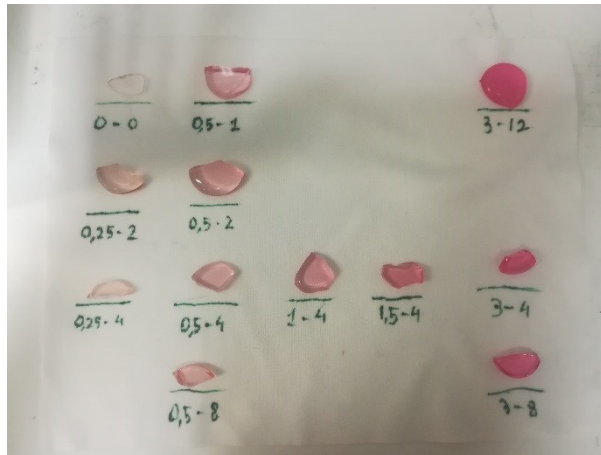


Figure 4-1: Picture of the borosilicate glasses prepared with different  $\text{Er}_2\text{O}_3$ - $\text{Yb}_2\text{O}_3$  contents (mole %)

While an increase in  $\text{Yb}_2\text{O}_3$  content has no impact on the color of the glasses, an increase in  $\text{Er}_2\text{O}_3$  leads to a darker pink coloration of the glasses

The density and thermal properties of the glasses are listed in Table 1.

Table 1: Density and thermal properties

Sample [ $\text{Er}_2\text{O}_3$ - $\text{Yb}_2\text{O}_3$ ] [mole %]	$\rho$ ( $\text{g}/\text{cm}^3$ ) [ $\pm 0.02\text{g}/\text{cm}^3$ ]	$T_g$ ( $^\circ\text{C}$ ) [ $\pm 3^\circ\text{C}$ ]	$T_x$ ( $^\circ\text{C}$ ) [ $\pm 3^\circ\text{C}$ ]	$\Delta T$ ( $^\circ\text{C}$ ) [ $\pm 6^\circ\text{C}$ ]
0-0	2.62	517	604	87
0.5-1	2.79	524	614	91
0.25-2	2.91	524	615	99
0.5-2	2.88	525	619	89
0.25-4	3.08	528	623	91
0.5-4	3.13	529	624	95
1-4	3.18	533	624	108
1.5-4	3.24	534	623	90
3-4	3.39	536	635	87
0.5-8	3.58	541	641	94
3-8	3.79	549	653	104

One can notice that  $\Delta T$ , the gauge of crystallization, is  $> 80^\circ\text{C}$  independently of the glass composition indicating that all glasses are good glass formers and so good candidates for the sintering process. No crystallization is expected to occur during the sintering process.

The density of the glasses as a function of the rare-earth (RE) content can be found in Fig: 4.2

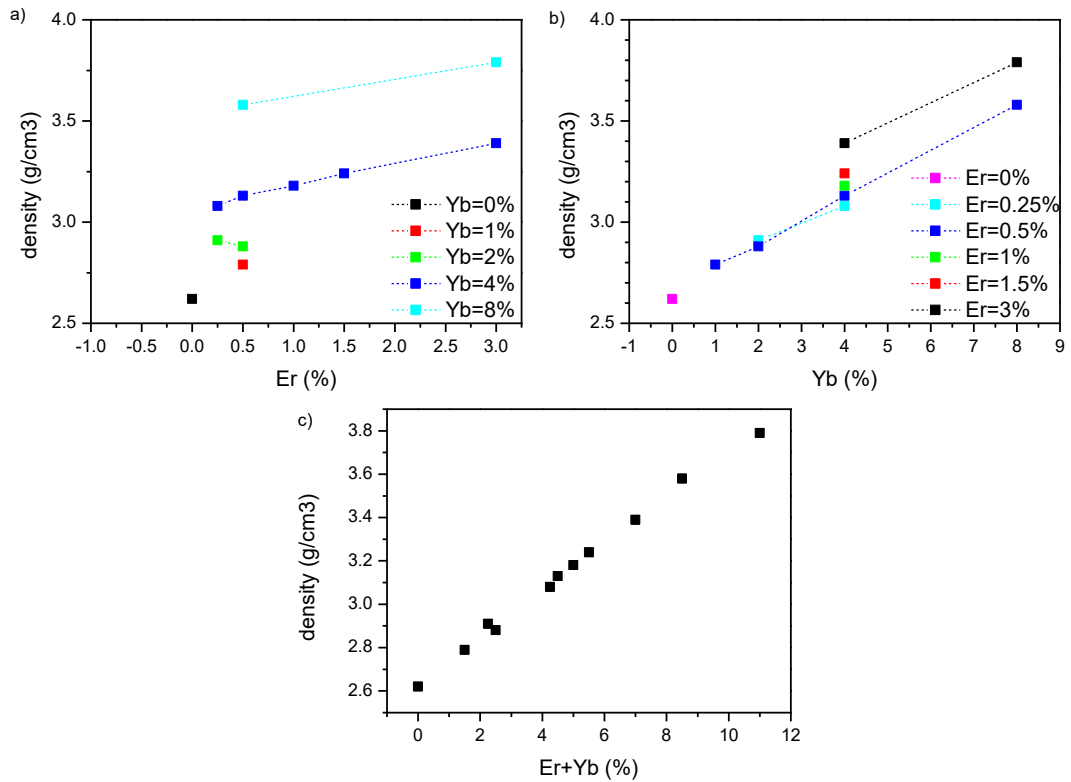


Figure 4-2 Density as a function of Er<sub>2</sub>O<sub>3</sub> (a), Yb<sub>2</sub>O<sub>3</sub> (b) and total RE content (c)

As observed in Fig: 4.2.a and b, an increase in the content of the RE ions in the glass increases the glass' density linearly. And as displayed in Fig: 4.2.c, the effect of both RE's ions has similarly strong effect on the increase in the density. This can be attributed to the addition of heavy ions increasing similarly the average density.

The thermal properties of the glasses as a function of the RE content can be found in Fig: 4.3

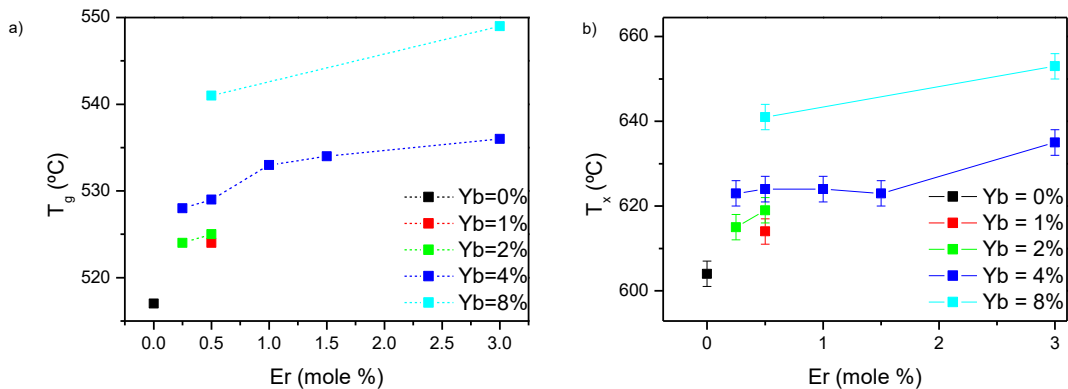


Figure 4-3: T<sub>g</sub> (a) and T<sub>x</sub> (b) as a function of Er<sub>2</sub>O<sub>3</sub> and Yb<sub>2</sub>O<sub>3</sub> content

While the progressive addition of Er<sup>3+</sup> has no significant impact on T<sub>g</sub> and T<sub>x</sub>, it is the progressive addition of Yb<sup>3+</sup> which increases T<sub>g</sub> and T<sub>x</sub>.

The absorption spectrum of the 0.5-4 glass, taken as an example, is shown in Fig: 4.4

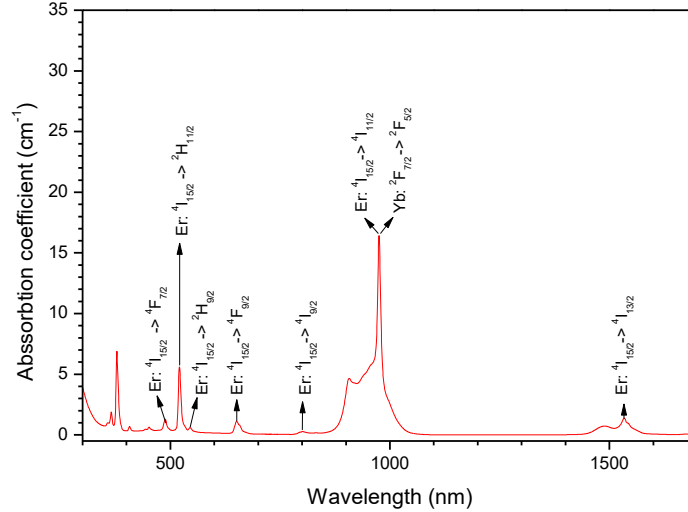


Figure 4-4: Absorption spectrum of the 0.5-4 glass.

The UV-Vis absorption spectrum on Fig: 4-4 exhibits multiple absorption bands related to the 4f-4f transitions of  $\text{Er}^{3+}$  from the ground state to the different excited levels. The absorption band at 980nm can also be related to the 4f-4f transition of  $\text{Yb}^{3+}$ .

The absorption coefficient and cross-sections of the investigated glasses are presented in Table 2.

Table 2: Absorption coefficients and cross-sections of the investigated glasses

Sample [ $\text{Er}_2\text{O}_3\%$ - $\text{Yb}_2\text{O}_3\%$ ]	[ $\text{Er}^{3+}$ ] ( $10^{20}$ ion. $\text{cm}^{-3}$ ) [ $\pm 4\%$ ]	[ $\text{Yb}^{3+}$ ] ( $10^{20}$ ion. $\text{cm}^{-3}$ ) [ $\pm 4\%$ ]	$\alpha$ (975nm) ( $\text{cm}^{-1}$ )	$\alpha$ (1534nm) ( $\text{cm}^{-1}$ )	$\sigma_{\text{abs}}$ (975nm) ( $10^{-21}\text{cm}^2$ ) [ $\pm 10\%$ ]	$\sigma_{\text{abs}}$ (1534nm) ( $10^{-21}\text{cm}^2$ ) [ $\pm 10\%$ ]
0.5-1	2.45	4.90	5.84	1.38	7.94	5.63
0.25-2	1.23	9.87	10.19	0.71	9.18	5.76
0.5-2	2.41	9.66	11.24	1.54	9.31	6.39
0.25-4	1.20	19.17	14.48	0.71	7.11	5.90
0.5-4	2.40	19.23	16.42	1.38	7.59	5.74
1-4	4.79	19.14	17.80	2.81	7.44	5.86
1.5-4	7.17	19.12	16.62	4.07	6.32	5.67
3-4	14.18	18.90	15.66	7.99	4.73	5.64
0.5-8	2.35	37.64	16.82	1.32	4.21	5.60
3-8	13.75	36.66	34.35	8.01	6.81	5.83

As expected, an increase in the  $\text{Er}_2\text{O}_3$  and  $\text{Yb}_2\text{O}_3$  content leads to an increase in the absorption coefficient at 975nm while the increase in the  $\text{Er}_2\text{O}_3$  content increases the absorption coefficient at 1534nm.

The absorption cross-sections are similar to the absorption cross-section of silicate glasses reported in [Fe, 10]. One can notice that the absorption cross-section at 1534 nm is independent of the RE content in the glass, suggesting that the  $\text{Er}^{3+}$  ions are located in the same sites in the investigated glasses. However, the absorption cross-section at 980nm depends on the RE content indicating that most probably the  $\text{Yb}^{3+}$  ions suffer changes in its electronic environment when the amount of rare-earth ions increases.

The upconversion spectra of the glasses were measured using 980nm pumping and some of the spectra are presented in Fig: 4-5.

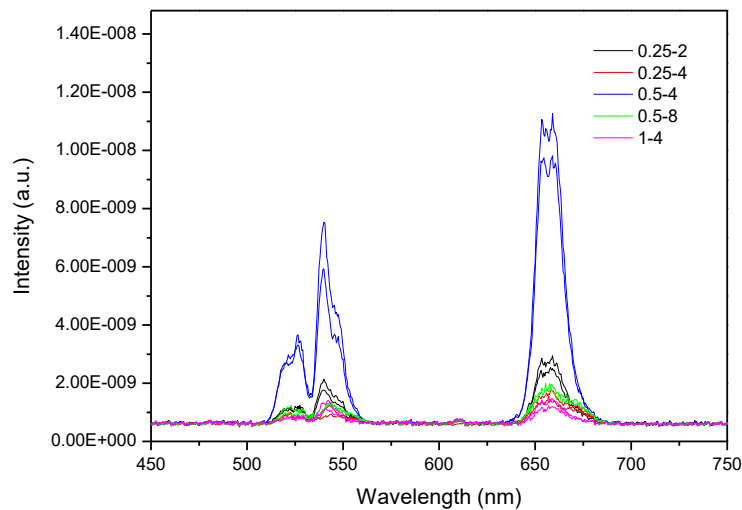


Figure 4-5: Up conversion spectra of selected glasses.

The spectra exhibit bands 526, 540 and 660nm which can be correlated to  $^2\text{H}_{11/2} \rightarrow ^4\text{I}_{15/2}$ ,  $^4\text{S}_{3/2} \rightarrow ^4\text{I}_{15/2}$  and  $^4\text{F}_{9/2} \rightarrow ^4\text{I}_{15/2}$  transitions of  $\text{Er}^{3+}$  ions, respectively [Br,93],[Li,08]. Unfortunately, the intensity of the red emission is larger than that of the green emission. Nonetheless, the glasses exhibit green upconversion. Additionally, one can notice that an increase of  $\text{Er}_2\text{O}_3$  and  $\text{Yb}_2\text{O}_3$  content from 0.25 to 0.5 and 2 to 4, respectively, increases the intensity of the upconversion. However, when the  $\text{Er}_2\text{O}_3$  and  $\text{Yb}_2\text{O}_3$  content further increase, the intensity of the upconversion decreases. As reported [Ti,12], the decrease in the intensity of the upconversion with an increase in the content of the rare-earth ions can be due to  $\text{Er}^{3+}$  concentration quenching, the energy transfer between  $\text{Er}^{3+}$  ions de-populating the thermalized levels  $^4\text{S}_{3/2}$ ,  $^2\text{H}_{11/2}$  and the level  $^4\text{F}_{9/2}$  of  $\text{Er}^{3+}$ .

*As a summary: due to its large intensity of the upconversion, the glass with 0.5 mol% of  $\text{Er}_2\text{O}_3$  and 4 mol% of  $\text{Yb}_2\text{O}_3$  (labeled at 0.5-4 glass) was chosen for the fabrication of the scaffold.*

#### 4.1.1.2 Fabrication and characterization of the $\text{Yb}^{3+}$ , $\text{Er}^{3+}$ doped scaffolds

To be considered as promising scaffolds, the scaffold should be possessed with a porosity of at least 65% and a compressive strength of 2-12MPa to be similar to that of cancellous bone [Fu,11]. The width of the bracket of possible values is due to the inherit

fluctuation of biological tissue, having properties that depend widely on the patient condition (age, fitness, sickness) and the specific bone.

The  $\text{Yb}^{3+}$ ,  $\text{Er}^{3+}$  doped scaffolds were sintered as explained in Chapter 3. The porosity of various scaffolds is shown in Fig: 4-6.

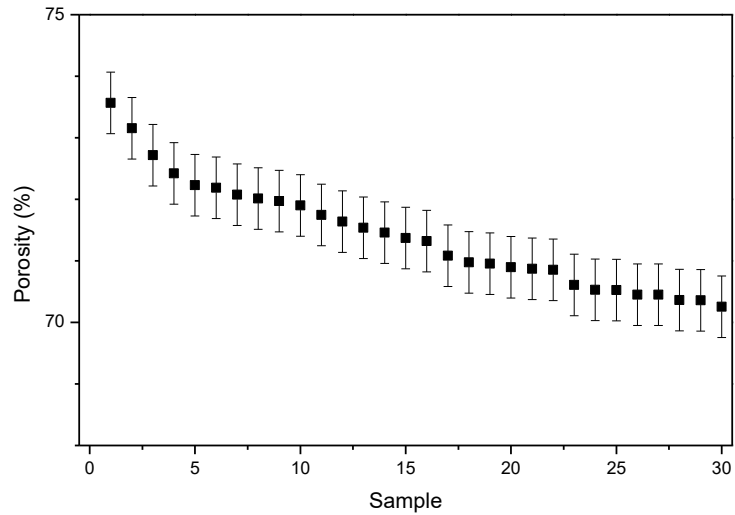


Figure 4-6: Porosity values of the different  $\text{Yb}^{3+}$ ,  $\text{Er}^{3+}$  codoped scaffolds.

Fig: 4-6 shows that scaffolds were successfully prepared with an average value of 71.42% porosity with a standard deviation of 0.87%.

Fig: 4-7 shows the compressive strength curve of one of the doped scaffolds showing that the compressing strength for this sample is  $\sim 0.9\text{MPa}$ .

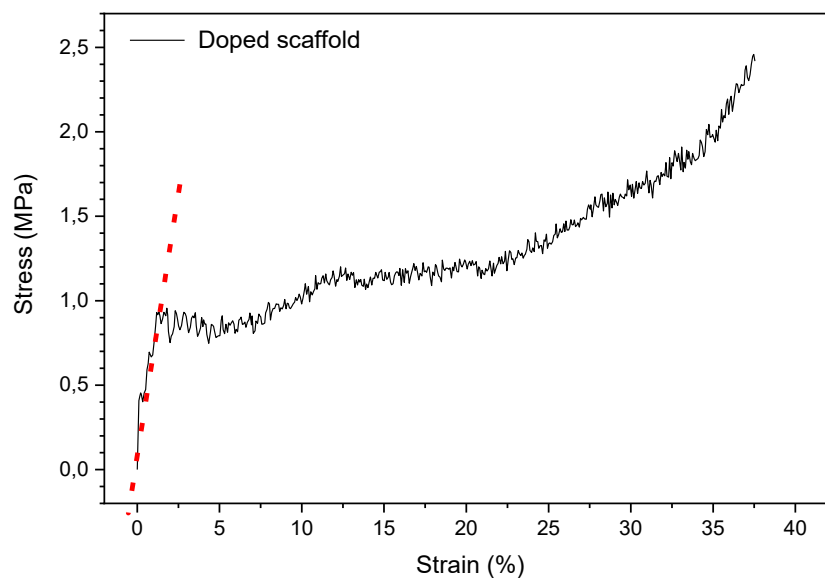


Figure 4-7: Compressive strength curve of a doped scaffold

The measurement was repeated for all scaffolds and the average compressive strength is estimated at  $(0.85 \pm 0.18)$  MPa which is lower compared to B50 scaffold measured at

2.5MPa for 50% porosity [Fa,17]. This reduction in the compressive strength should be related to different porosities of the scaffolds. However, one should point out that the test performed here is not reliable due to the poor sample preparation (parallelization and polishing of the scaffolds). The measurements should be repeated. Nonetheless, the scaffolds possess suitable porosity and acceptable level of mechanical properties.

The upconversion spectra of the scaffolds were measured in different areas in a scaffold and in different scaffolds in order to check the homogeneity of the upconversion intensity within one scaffold and between the scaffolds. The upconversion spectra are shown in Fig: 4-8a.

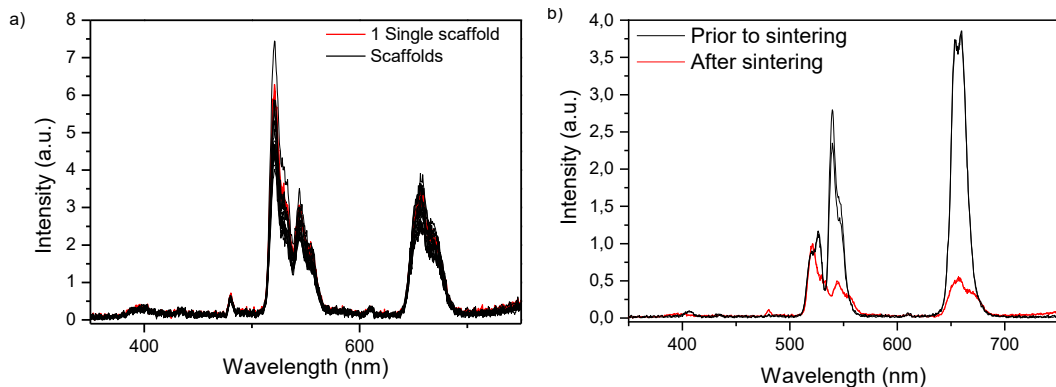


Figure 4-8: Upconversion spectra of scaffolds (a) and of the glass prior to and after sintering. (b)

As shown in Fig: 4.8a, the scaffold exhibits uniform intensity of upconversion when measured in different parts of the scaffold. One can also notice the good homogeneity in the intensity of the upconversion between the scaffolds confirming that it is possible to process a large number of scaffolds with homogenous upconversion. As compared to the data presented in Fig: 4-5, the signal is noisier due to lower intensity of upconversion. This is due to the lower amount of glass (and so to the amount of RE) when performing the measurement on the porous scaffolds. As shown in Fig: 4.8b, the upconversion spectrum is modified after the sintering process indicating that the sites of  $\text{Er}^{3+}$  change after sintering.

In order to understand the changes in the upconversion spectra, the XRD pattern of the scaffold was measured and can be found in Fig: 4-9.

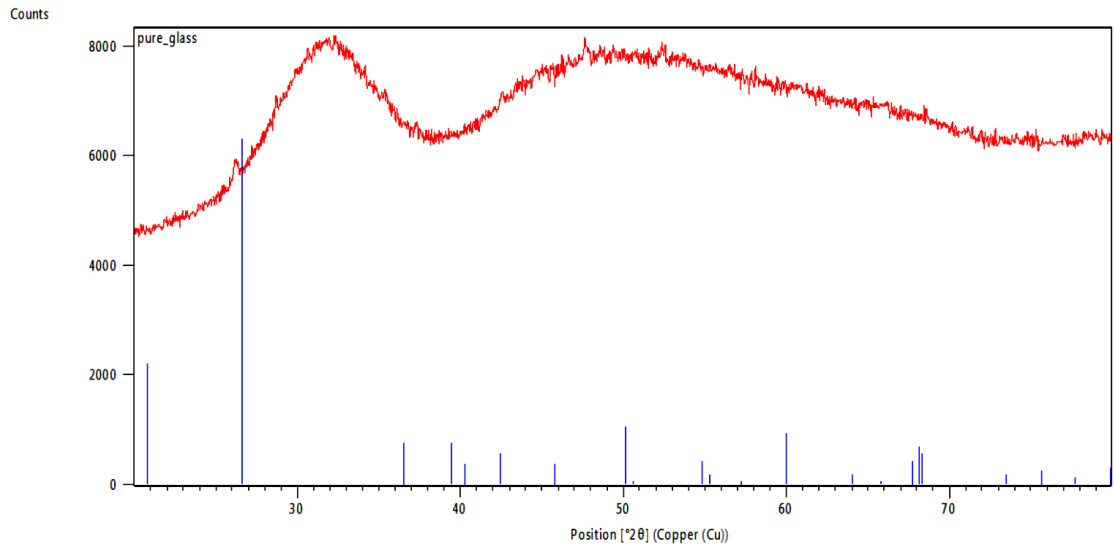


Figure 4-9: XRD pattern of the Yb<sup>3+</sup>, Er<sup>3+</sup> doped scaffold

Surprisingly, sharp peaks with small intensity can be seen in the Yb<sup>3+</sup>, Er<sup>3+</sup> doped scaffold revealing the presence of crystals in the scaffolds, the identification of which is still in progress. It is maybe the partial crystallization of the scaffolds which leads to changes in upconversion properties. The partial crystallization of the Yb<sup>3+</sup>, Er<sup>3+</sup> doped glass during sintering is not understood as this glass was found to be thermally stable.

#### 4.1.2 Scaffold preparation with NaYF<sub>4</sub>: Yb<sup>3+</sup>, Er<sup>3+</sup> nanocrystals

Scaffolds with NaYF<sub>4</sub>: Yb<sup>3+</sup>, Er<sup>3+</sup> nanocrystals (NCs) were also fabricated using the sintering process by adding the NCs in the glass crushed into powder prior to sintering.

At first, the amount of the NCs was optimized in order to tailor the amount of NCs to process scaffolds with strong upconversion while possessing the required properties listed in the previous section. The porosity and the mechanical properties of the scaffolds prepared with different weight % of the NCs are shown in Fig: 4.10.

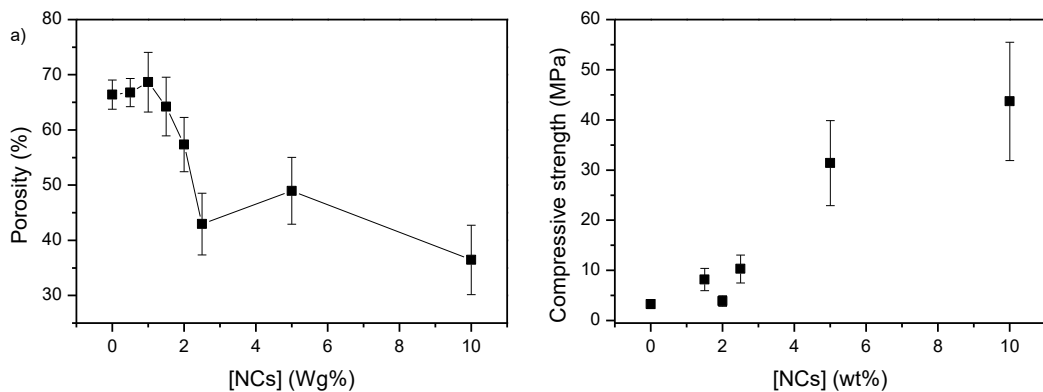


Figure 4-10: Porosity and compressive strength curve of NCs containing scaffolds.

An increase in the amount of NCs decreases the porosity of the scaffold and so increases the compression strength. As expected, the intensity of the conversion was found to increase as the amount of NCs increases. We also found out that it is difficult to prepare scaffolds with homogeneous upconversion when adding the NCs in low amount. Therefore, the amount of NCs was fixed at 2wt%. The scaffolds have a porosity of  $(57,4 \pm 4.9) \%$ . Due to their low porosity, the scaffolds have a compressive strength of  $(3.9 \pm 1.1)$  MPa which is higher than that of the measured in the B50 scaffolds.

The up-conversion spectra of the NCs containing scaffolds were measured. The upconversion spectra of the as-prepared NCs and of the NCs containing scaffolds are presented in Fig: 4-11.

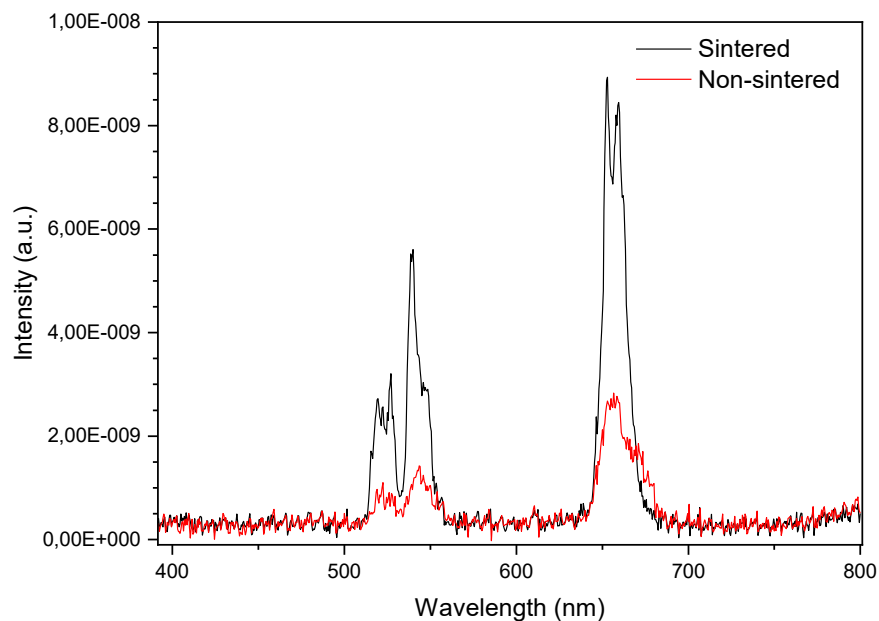


Figure 4-11: Comparison between up conversion spectra of NC containing scaffolds before and after sintering

It is clearly shown that the sintering process has an impact on the upconversion spectrum.

In order to understand this result, all intermediate sintering states were individually tested (heat treatment & grinding) for the nanocrystals alone and the results are displayed in Fig 4-12.

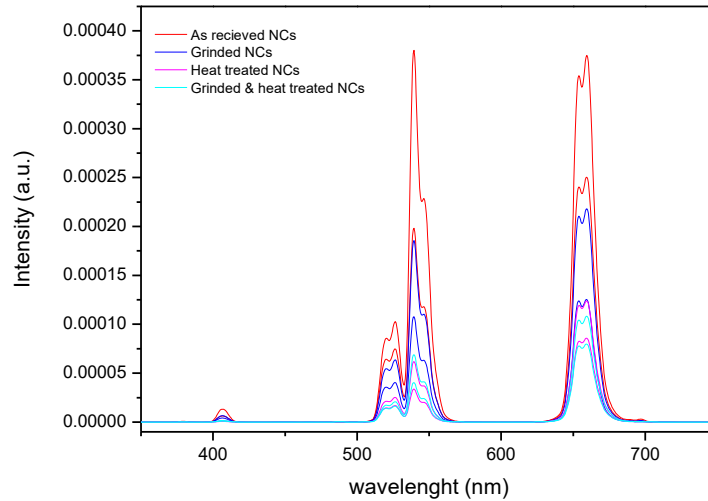


Figure 4-12 NCs alone UC spectrum prior to and after sintering

Fig 4-11 shows that both heat treatment and mechanical grinding lead to a reduction in the up-conversion emission of the nanocrystals with an increase of the red to green ratio. This could be attributed to a change in the crystalline structure of the nanocrystals promoted by the external energy applied, changing from hexagonal to high temperature cubic phase as reported in [Ha, 11], [Hy, 16]. However, in our study, the sintering temperature is too low to induce any changes in the crystalline structure. It is possible that the decrease in the upconversion after sintering is related to the thermal activation of the deleterious thermal phonons from host lattice, internal/surface crystalline defects and surface chemical bonds in agreement with [Ya, 19]. The grinding is then expected to create inter defects which might cause the intensity of the upconversion to decrease.

The XRD pattern of the NCs containing scaffold which contains 10wt% of NCs is displayed in Fig 4-13.

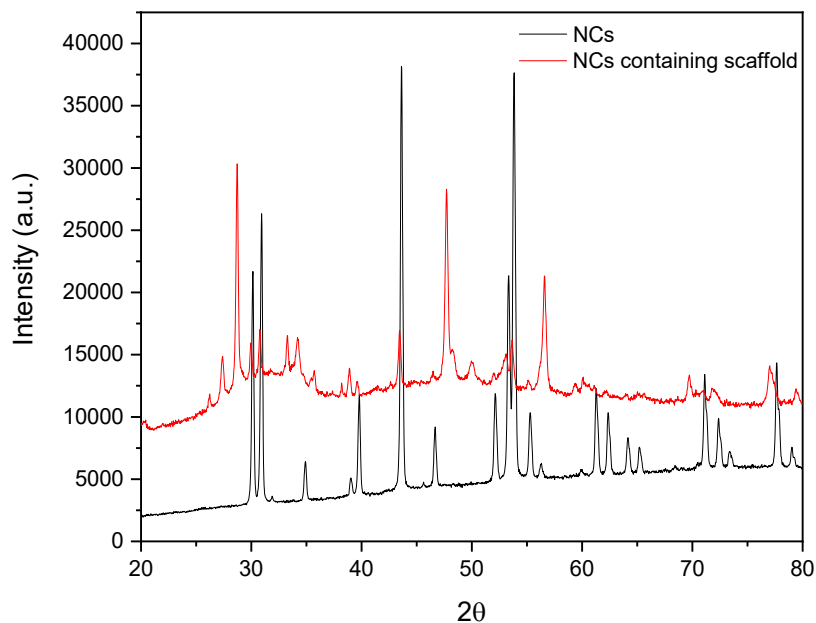


Figure 4-13 XRD pattern of the 10wt% NCs containing scaffolds and of the NCs alone

The XRD pattern of the NCs containing scaffold shows peaks which can be related to the NCS. However, as seen in Fig: 4-13, additional peaks can be observed indicating the presence of additional crystals in the glass as seen for the doped scaffolds.

The NCs scaffolds were investigated under SEM to verify how the NCs are distributed in the scaffold. Fig: 4-14 shows the SEM pictures of the NCs containing scaffold which contain 2wt% of NCs.

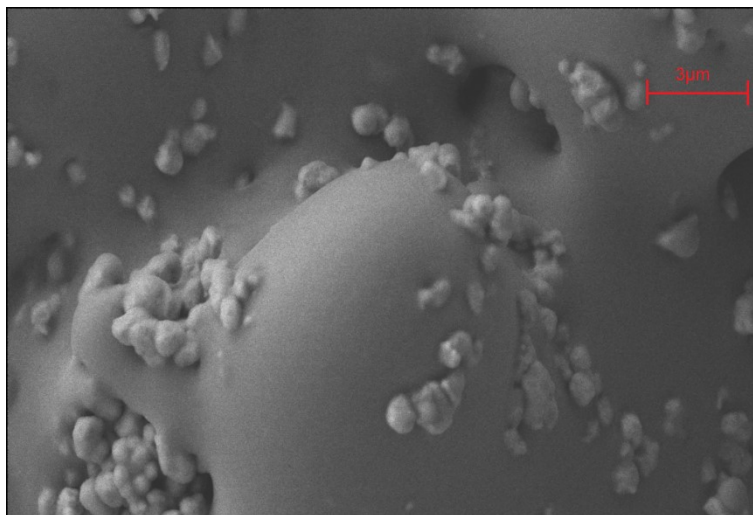


Figure 4-14: SEM pictures of the NCs scaffolds:

As shown above, the NCs are agglomerated with a size of 500-1000nm. The agglomerates were found to be well dispersed. No crystals could be seen using SEM.

The elemental mapping can be found in Fig: 4-15.

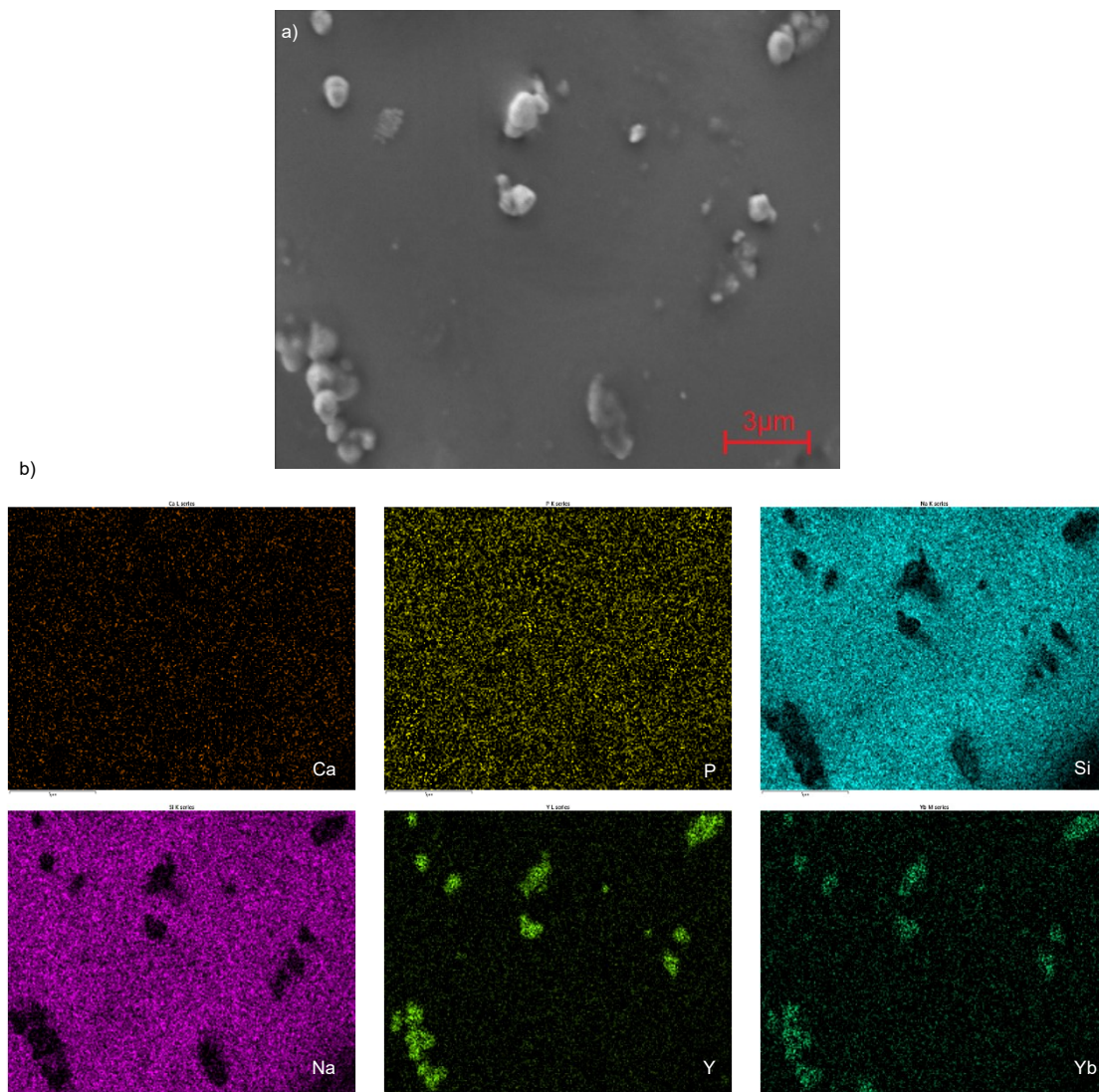


Figure 4-15: SEM image (a) and elemental EDS mapping (b) of the NCs containing scaffold

The elemental mapping allowed one to see clearly the NCs. The composition around the NCs is homogeneous. No crystals could be suspected neither from the elemental mapping.

## 4.2 Photocleavage of molecules using NIR pumping

In this section, we first present the in-vitro testing of the newly developed scaffolds and then the preliminary results of the photocleavage of molecules using UV and green light.

### 4.2.1 In vitro testing

The different scaffolds were tested in vitro using simulated body fluid (SBF), for up to 2 weeks. During incubation the samples were placed in a shaking incubator (120 RPM), at 37°C. The SBF/glass ratio used for the experiments was 10mL/100mg.

The mass loss of the scaffolds and the change of pH in the SBF were measured over time and their results are summarized in Fig: 4-16.

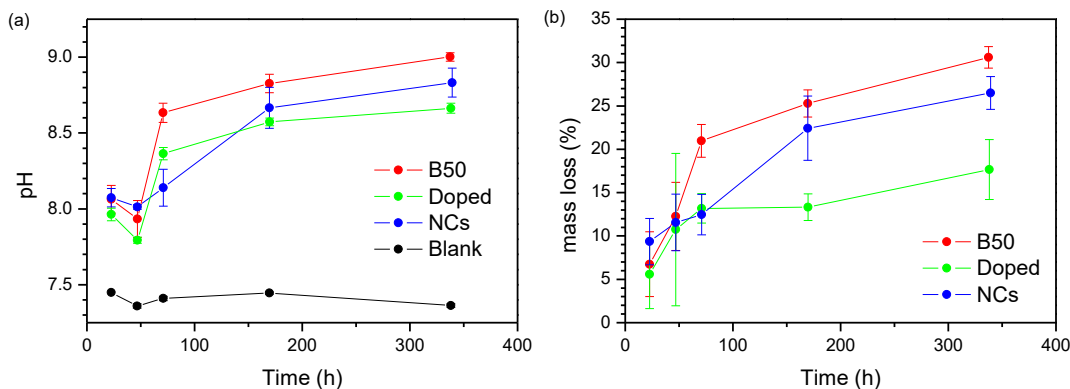


Figure 4-16: pH of the immersion solution (a) and scaffolds mass loss (b) as a function of immersion time in SBF. The undoped scaffolds are labelled as “B50”, the  $\text{Er}^{3+}$ ,  $\text{Yb}^{3+}$ , codoped scaffolds as “Doped”, and the  $\text{NaYF}_4: \text{Yb}^{3+}, \text{Er}^{3+}$  nanocrystals containing scaffolds as “NCs”. A blank sample (only SBF) is also displayed, to show the variation in pH of the buffering solution, as a function of incubation time.

The pH of the solutions which contains the scaffolds increases overtime due to the release of alkaline and alkaline earth ions from the glass to the solution increasing the basicity of the solution [Se,00] [He,06]. One can notice that the solutions with the newly developed scaffolds (doped and NCs) have lower pH than the solution which contains the well-known B50 scaffold although the glass matrix to prepare the scaffolds is the same.

In Fig: 4-16 (b), a similar behavior can be observed: the mass loss increases with immersion time in SBF and can be related to the dissolution rate [Hu,06]. The newly developed scaffolds exhibit a smaller mass loss than the reference B50 scaffold indicating that they possess a slower dissolution rate than the reference B50 scaffold. It is clearly shown that the addition of  $\text{Er}^{3+}$  and  $\text{Yb}^{3+}$  in the glass reduces more the dissolution rate of the glass than adding the NCs in the glass. This may be due to the partial crystallization of the scaffolds and/or to the different glass structures, clearly showing the need to investigate the structure of the glass.

### 4.2.2 Drug released using 980nm excitation

The possibility of the scaffolds to promote changes in an organic molecule was tested using Phthalimide-Azo-Iperoxo (PAI). This molecule shows a trans-cis isomer reversible switching promoted by light interaction:

- when irradiated with high energy photons (peak absorption at 315nm), the trans to cis switching is promoted,
- when irradiated with photons of lower energy (green light), the cis to trans switching is promoted.[Ri,19]

The trans-cis switch can be tracked from the changes in the absorption spectrum of the molecules. 1mg of the molecule was diluted in 42.6ml of SBF and placed in a quartz cuvette. Fig: 4-17 presents the absorption spectrum of the as-prepared solution.

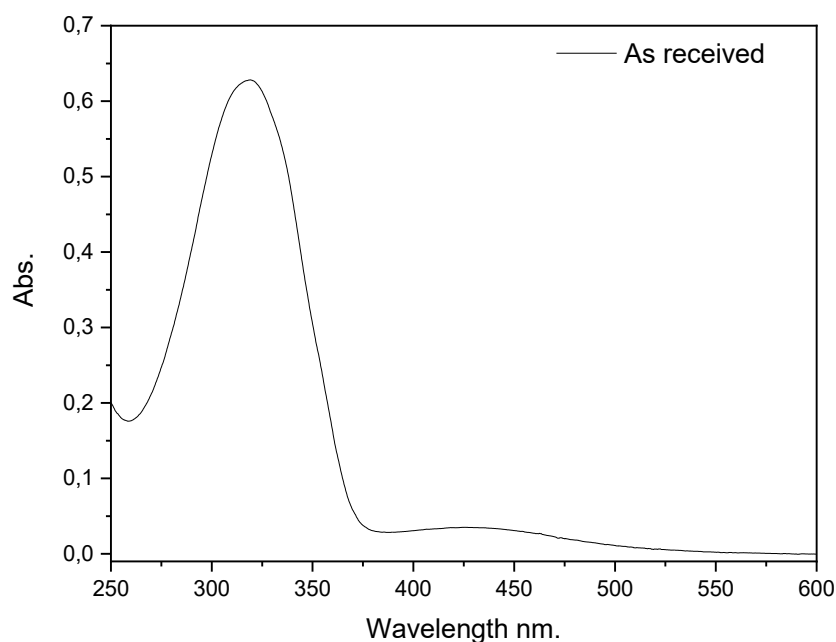


Figure 4-17: Absorption spectrum of as received PAI molecule

The absorption spectrum exhibits 2 absorption bands at 319 and 426 nm which can be related to trans and cis isomerism, respectively.

The switching of the molecule was tested using a 365nm UV lamp. The solution was irradiated from the top and from the side of the cuvette for 5min to few hours and the absorption spectra are shown in Fig: 4-18a and b, respectively.

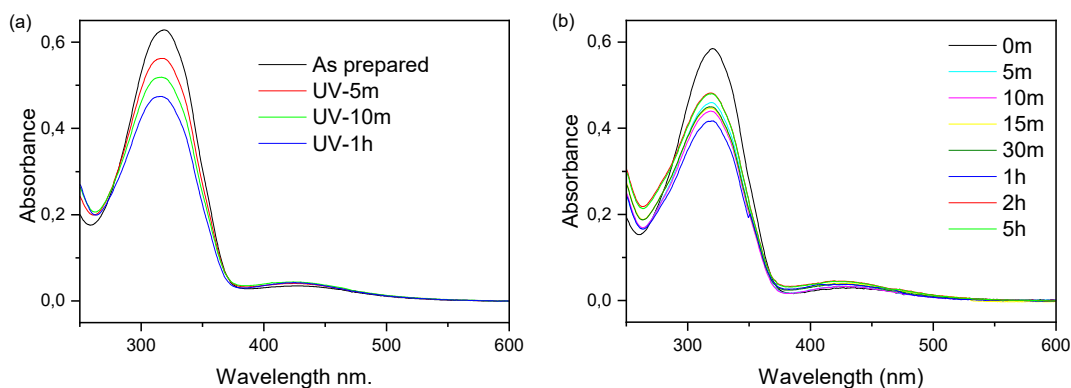


Figure 4-18: Absorption spectrum of PAI solution in SBF irradiated with UV lamp from the top (a) and from the side (b)

As shown above, it is possible to reduce the intensity of the band at 319nm, related to trans, using UV lamp. The irradiation is more efficient when irradiating the cuvette from the side. Therefore, it is possible to reduce by 25% the intensity of the absorption band when irradiating from the side for 1 hour.

The solution was also irradiated with a green laser pointer. The absorption spectrum was measured after 5 and 15min irradiation.

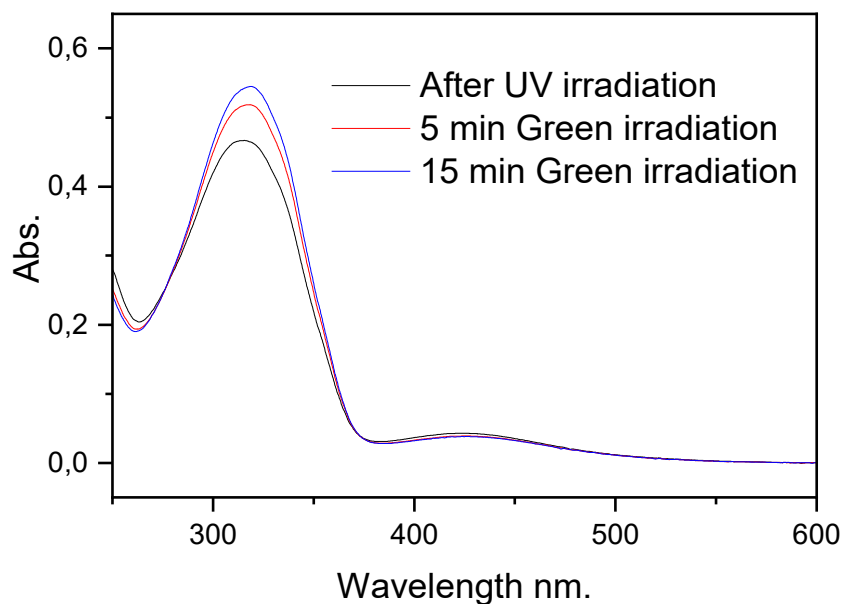


Figure 4-19 Absorption spectrum of PAI solution in SBF after irradiation with green light

An increase in the intensity of the absorption band at 319nm increases after green irradiation, as shown in Fig:4-19, this increase is larger when the duration of the green irradiation is longer. This clearly shows that the green laser pointer can be used to convert back the molecule to trans isomerism.

## 5. CONCLUSIONS

In this work, new biophotonics scaffolds have been developed so they can be used as an externally controlled localized drug delivery system (DDS) when loaded with photochromic drug. The glass of investigation was the well-known B50 bioactive glass in which  $\text{Er}^{3+}$  and  $\text{Yb}^{3+}$  ions were added to add some luminescence properties. In this study, two different approaches were used to fabricate: the scaffolds were prepared by adding the RE ions in the glass and scaffolds were prepared with the upconverter  $\text{NaYF}_4: \text{Yb}^{3+}, \text{Er}^{3+}$  crystals. We clearly showed that it is possible to prepare these scaffolds with proper porosity, acceptable compression strength and green upconversion. However, crystallization was found to occur during sintering. In vitro testing of the scaffolds has been produced and compared to the base B50 biocompatible glass, and the results were into acceptable range. The active scaffolds were found to have a slower dissolution rate than the B50 glass probably due to the partial crystallization and/or to different structures of the scaffolds. A photoswitchable molecule was characterized to be used as a sensor and trigger of the drug release in the DDS.

### Next steps to be made in the scope of this project:

Due to the outbreak of the COVID-19 pandemic, and the resulting closure of university facilities, the following measurements couldn't be performed

- **Mechanical properties characterization of doped scaffolds** should be measured
- **Mechanical properties characterization of scaffolds after immersion** should be measured.
- **Crystalline phases identification in scaffolds:** A throughout investigation of the different crystalline phases present in the newly developed scaffolds should be studied to understand how to suppress the formation of crystalline phases. The recommended procedure would be a complete analysis of the XRD spectrum, to properly identify all peaks.
- **Up conversion measurement of the immersed scaffolds:** The upconversion luminescence of the immersed scaffolds should be measured and compared to that of the samples prior to immersion to confirm that the scaffolds still exhibit green upconversion while being covered by the hydroxyl apatite layer forming during the immersion in SBF.
- **Ion release during SBF immersion:** Samples from the incubation of scaffolds in SBF have been stored in the refrigerator for ICP measurements, in order to identify the ions present in the solution and their concentrations. This experiment would provide useful information about the biocompatibility and degradation rate of the scaffolds.
- **Activation of the photoswitchable molecule with the upconverter scaffolds:** a proper characterization of the upconverter scaffolds loaded with the photoswitchable molecule solution should be performed to check if the green upconversion from the scaffolds could be used to photocleave the molecule.

With these measurements, we expect to be able to identify which scaffold is the most promising to be used as a DDS.

## **Next steps outside of the scope of the project**

- **Creation of a light sensitive drug reservoir:** The main idea of the project relies on the ability of breaking the surface layer of a sensitive drug reservoir using light. One of the main challenges of this project is the fabrication of said reservoir. As the skills required for this step are different to those of the rest of the study, this part is left for a future collaboration with a chemistry center research group.
- **Optimization of the material combination and production methods:** This thesis purpose was to prove the concept, but a better optimization of the photosensitive molecule and upconverter pair should be performed to better match the absorbance/emission spectra of each other, to provide a more efficient cleavability of the drug reservoir.

## 6. REFERENCES

- [Al,04] Allen, T M., and Pieter R. Cs. 2004. "Drug Delivery Systems: Entering the Mainstream." *Science* 303(5665): 1818–22. <https://www.sciencemag.org/lookup/doi/10.1126/science.1095833> (March 26, 2020).
- [Al,12] Altenaiji, M, Schleyer, G K and Zhao, Y Y. 2012. "Characterisation of Aluminium Matrix Syntactic Foams Under Static and Dynamic Loading." <http://dx.doi.org/10.5772/48560> (March 16, 2020).
- [Be,13] Bergmann, C P., and Aisha, S. 2013. Dental Ceramics: Microstructure, Properties and Degradation *Dental Ceramics: Microstructure, Properties and Degradation*. Springer Berlin Heidelberg.
- [Br,93] Brede, R.. 1993. "Green Up-Conversion Laser Emission in Er-Doped Crystals at Room Temperature." *Applied Physics Letters* 63(15): 2030–31. <http://aip.scitation.org/doi/10.1063/1.110581> (March 16, 2020).
- [Ch,01] Chatterjee, A.K. 2001. Handbook of Analytical Techniques in Concrete Science and Technology *Handbook of Analytical Techniques in Concrete Science and Technology*. Elsevier. <http://www.sciencedirect.com/science/article/pii/B9780815514374500114> (March 25, 2020).
- [Ch,02] Chen, G, Takashi U, and Tetsuya T. 2002. "Scaffold Design for Tissue Engineering." *Macromolecular Bioscience* 2(2): 67–77.
- [De,15] Deliormanli, A M. 2015. "Preparation and in Vitro Characterization of Electrospun 45S5 Bioactive Glass Nanofibers." *Ceramics International* 41(1): 417–25.
- [De,06] Deville, S, Saiz, E, and Antoni P. T. 2006. "Freeze Casting of Hydroxyapatite Scaffolds for Bone Tissue Engineering." *Biomaterials* 27(32): 5480–89.
- [Do,09] Domachuk, P. 2009. "Bioactive 'Self-Sensing' Optical Systems." *Applied Physics Letters* 95(25): 253702. <http://aip.scitation.org/doi/10.1063/1.3275719> (April 2, 2020).
- [Ep,16] Epp, J. 2016. "X-Ray Diffraction (XRD) Techniques for Materials Characterization." In *Materials Characterization Using Nondestructive Evaluation (NDE) Methods*, Elsevier Inc., 81–124.
- [Fa,17] Fabert, M. 2017. "Crystallization and Sintering of Borosilicate Bioactive Glasses for Application in Tissue Engineering." *Journal of Materials Chemistry B* 5(23): 4514–25.
- [Fa,12] Fagerlund, S, Hupa, L and Hupa, M. 2012. *Understanding the in Vitro Dissolution Rate of Glasses with Respect to Future Clinical Applications*.
- [Fe,10] Feng, Z 2010. "Er<sup>3+</sup>-Yb<sup>3+</sup> Codoped Borosilicate Glass for Optical Thermometry." *Science China: Physics, Mechanics and Astronomy* 53(5): 848–51. <https://doi.org/10.1007/s11433-010-0188-9>.
- [Fi,20] Fiberlabs, Inc. 2020. "Stimulated and Spontaneous Emission | Fiberlabs

Inc.” <https://www.fiberlabs.com/glossary/stimulated-emission/> (March 30, 2020).

- [Fu,10] Fu, Q., Rahaman, M N, Hailuo F, and Xin L. 2010. “Silicate, Borosilicate, and Borate Bioactive Glass Scaffolds with Controllable Degradation Rate for Bone Tissue Engineering Applications. I. Preparation and in Vitro Degradation.” *Journal of Biomedical Materials Research Part A* 95A(1): 164–71. <http://doi.wiley.com/10.1002/jbm.a.32824> (March 20, 2020).
- [Fu,11] Fu, Q, Saiz, E., Rahaman, M N, and Antoni P. T. 2011. “Bioactive Glass Scaffolds for Bone Tissue Engineering: State of the Art and Future Perspectives.” *Materials Science and Engineering C* 31(7): 1245–56. <https://linkinghub.elsevier.com/retrieve/pii/S0928493111001275> (March 24, 2020).
- [Fu,11 (2)] Fu, Q, Saiz, E, and Antoni P. T. “Bioinspired Strong and Highly Porous Glass Scaffolds.” *Advanced Functional Materials* 21(6): 1058–63. <http://doi.wiley.com/10.1002/adfm.201002030> (March 31, 2020).
- [Ga,06] Gan, F., and Lei X. 2006. *Photonic Glasses*. World Scientific.
- [Go,12] Goldstein, J. 2012. *Scanning Electron Microscopy and X-Ray Microanalysis: Third Edition*. Boston, UNITED STATES: Springer. <http://ebookcentral.proquest.com/lib/tampere/detail.action?docID=1255339>.
- [Go,01] Gong, W, Abdesselam A, and Werner L. 2001. “Porous Bioactive Glass and Glass–Ceramics Made by Reaction Sintering under Pressure.” *Journal of Biomedical Materials Research* 54(3): 320–27.
- [Ha,11] Harju, E. 2011. “Polymorphism of NaYF<sub>4</sub>:Yb<sup>3+</sup>, Er<sup>3+</sup> Up-Conversion Luminescence Materials.” *Zeitschrift für Kristallographie Proceedings* 1(1): 381–87. [https://www.researchgate.net/publication/234107487\\_Polymorphism\\_of\\_NaYF4Yb3\\_Er3\\_Up-Conversion\\_Luminescence\\_Materials](https://www.researchgate.net/publication/234107487_Polymorphism_of_NaYF4Yb3_Er3_Up-Conversion_Luminescence_Materials).
- [He,14] Hemmer, E, Fiorenzo V, and Kohei S. 2014. “Lanthanide-Based Nanostructures for Optical Bioimaging: Small Particles with Large Promise.” *MRS Bulletin* 39(11): 960–64.
- [He,71] Hench, L. L., R. J. Splinter, W. C. Allen, and T. K. Greenlee. 1971. “Bonding Mechanisms at the Interface of Ceramic Prosthetic Materials.” *Journal of Biomedical Materials Research* 5(6): 117–41.
- [He,91] Hench, L L. 1991. “Bioceramics: From Concept to Clinic.” *Journal of the American Ceramic Society* 74(7): 1487–1510. <http://doi.wiley.com/10.1111/j.1151-2916.1991.tb07132.x> (March 30, 2020).
- [He,06] Hench, L. L 2006. “The Story of Bioglass®.” In *Journal of Materials Science: Materials in Medicine*, Springer, 967–78. <http://link.springer.com/10.1007/s10856-006-0432-z> (March 27, 2020).
- [Ho,05] Hollister, S J. 2005. “Porous Scaffold Design for Tissue Engineering.” *Nature Materials* 4(7): 518–24.
- [Hu,06] Huang, W; Rahaman, M N.; Day, D E.; Li, Y. 2006. “Mechanisms for Converting Bioactive Silicate, Borate, and Borosilicate Glasses to Hydroxyapatite in Dilute Phosphate Solution.” *Phys & Chemistry of Glasses: Eur. J. Sci. Technol. B.* 47: 647-658 (12).
- [Hu,12] Huang, S. 2012. “Electrospinning Preparation and Drug Delivery Properties

of  $\text{Eu}^{3+}/\text{Tb}^{3+}$  Doped Mesoporous Bioactive Glass Nanofibers." *Journal of Colloid and Interface Science* 387(1): 285–91.

- [Hy,16] Hyppänen, I. 2016. "Preparation and Up-Conversion Luminescence Properties Of." : 254–58.
- [Je,15] Jena, S, R B, Tokas, S T, and Sahoo, N K. 2015. "Characterization of Optical Thin Films by Spectrophotometry and Atomic Force Microscopy." *SMC Bulletin* 6(1): 1–9.
- [Jo,15] Jones, J R. 2015. "Reprint of: Review of Bioactive Glass: From Hench to Hybrids." *Acta Biomaterialia* 23(S): S53–82.
- [Ki,11] Kim, J W, and Du G M. 2011. "Basic Principles of Laser for Prostate Surgery." *Korean Journal of Andrology* 29(2): 101.
- [Ko,90] Kokubo, T. 1990. "Solutions Able to Reproduce in Vivo Surface-Structure Changes in Bioactive Glass-Ceramic A-W3." *Journal of Biomedical Materials Research* 24(6): 721–34. <http://doi.wiley.com/10.1002/jbm.820240607> (March 20, 2020).
- [Ko,06] Kokubo, T, and Hiroaki T. 2006. "How Useful Is SBF in Predicting in Vivo Bone Bioactivity?" *Biomaterials* 27(15): 2907–15.
- [Le,10] Lee, P I, and Li, J X. 2010. "Evolution of Oral Controlled Release Dosage Forms." In *Oral Controlled Release Formulation Design and Drug Delivery*, John Wiley & Sons, Ltd, 21–31. <https://onlinelibrary.wiley.com/doi/abs/10.1002/9780470640487.ch2>.
- [Li,08] Li, C. 2008. "Significant Temperature Effects on Up-Conversion Emissions of  $\text{Nd}^{3+}:\text{Er}^{3+}:\text{Yb}^{3+}$  Co-Doped Borosilicate Glass and Its Thermometric Application." *Sensors and Actuators, B: Chemical* 134(1): 313–16.
- [Li,07] Li, X. 2007. "Hierarchically Porous Bioactive Glass Scaffolds Synthesized with a PUF and P123 Cotemplated Approach." *Chemistry of Materials* 19(17): 4322–26.
- [Li,10] Lindfors, N C. 2010. "A Prospective Randomized 14-Year Follow-up Study of Bioactive Glass and Autogenous Bone as Bone Graft Substitutes in Benign Bone Tumors." *Inc. J Biomed Mater Res Part B: Appl Biomater* 94: 157–64. [www.interscience.wiley.com](http://www.interscience.wiley.com) (March 30, 2020).
- [Ma,04] Ma, P X. 2004. "Scaffolds for Tissue Fabrication." *Materials Today* 7(5): 30–40. <https://linkinghub.elsevier.com/retrieve/pii/S1369702104002330> (March 26, 2020).
- [Ma,12] Massera, J, Fagerlund, S, Hupa, L and Hupa. M 2012. "Crystallization Mechanism of the Bioactive Glasses, 45S5 and S53P4" ed. L. Pinckney. *Journal of the American Ceramic Society* 95(2): 607–13. <http://doi.wiley.com/10.1111/j.1551-2916.2011.05012.x> (March 31, 2020).
- [Mi,20] Minbos, Resources Limited. 2020. "Rare Earths - Minbos Resources Limited." <http://minbos.com/rare-earths/> (March 30, 2020).
- [Mi,04] Mio, H, Junya K, Fumio S, and Kantaro K. 2004. "Optimum Revolution and Rotational Directions and Their Speeds in Planetary Ball Milling." *International Journal of Mineral Processing* 74: S85–92.

<https://www.sciencedirect.com/science/article/pii/S0301751604000274> (February 12, 2020).

- [Oj,18] Ojansivu, M. 2018. "The Effect of S53P4-Based Borosilicate Glasses and Glass Dissolution Products on the Osteogenic Commitment of Human Adipose Stem Cells." *PLoS ONE* 13(8).
- [Oj,16] Ojha, N. 2016. "Borosilicate Glass With Enhanced Hot Forming." (February).  
<http://dspace.cc.tut.fi/dpub/bitstream/handle/123456789/24187/Ojha.pdf?sequence=1>.
- [Ol,98] Oliveira, A. S.. 1998. "Frequency Upconversion in Er<sup>3+</sup>/Yb<sup>3+</sup>-Codoped Chalcogenide Glass." *Applied Physics Letters* 72(7): 753–55.  
<http://aip.scitation.org/doi/10.1063/1.120884> (March 30, 2020).
- [Pa,16] Palo, E. 2016. "Up-Conversion Luminescence of the NaYF<sub>4</sub>:Yb<sup>3+</sup>,Er<sup>3+</sup> Nanomaterials Prepared with the Solvothermal Synthesis." *Optical Materials* 59: 49–54. <http://dx.doi.org/10.1016/j.optmat.2016.02.043>.
- [Ph,13] PHYSICS, INSTITUTE FOR NUCLEAR AND RADIATION. 2013. "X-Ray Diffraction – Bruker D8 Discover – Institute for Nuclear and Radiation Physics." <https://fys.kuleuven.be/iks/nvsf/experimental-facilities/x-ray-diffraction-2013-bruker-d8-discover> (March 30, 2020).
- [Pr,18] Prasad S., Sakthi. 2018. "Effect of Boron Oxide Addition on Structural, Thermal, in Vitro Bioactivity and Antibacterial Properties of Bioactive Glasses in the Base S53P4 Composition." *Journal of Non-Crystalline Solids* 498: 204–15.
- [Ra,11] Rahaman, M N. 2011. "Bioactive Glass in Tissue Engineering." *Acta Biomaterialia* 7(6): 2355–73.
- [Ri,19] Riefolo, F. 2019. *Optical Control of Cardiac Function with a Photoswitchable Muscarinic Agonist*.  
<https://pubs.acs.org/doi/abs/10.1021/jacs.9b03505> (March 4, 2020).
- [Ro,18] Roldán del Cerro, P. 2018. "Silicate and Phosphate Biophotonic Glasses." *Universidad Politécnica de Madrid Escuela Técnica Superior de Ingenieros de Caminos, Canales y Puertos*.
- [Se,00] Sepulveda, P, Julian, R J, and Hench, L L. 2000. "Effect of Particle Size on Bioglass® Dissolution." *Key Engineering Materials* 192–195: 629–34.  
<https://www.scientific.net/KEM.192-195.629>.
- [Ni,20] Services, U.S. Department of Health & Human, and National Institutes of Health. "Biomaterials." <https://www.nibib.nih.gov/science-education/science-topics/biomaterials> (March 20, 2020).
- [Sh,05] Shelby, J E. 2005. 208 The Royal Society of Chemistry *Introduction to Glass Science and Technology*.
- [Si,12] Siepmann, J, Ronald A. S, and Michael J. R. 2012. Fundamentals and Applications of Controlled Release Drug Delivery *Fundamentals and Applications of Controlled Release Drug Delivery*. eds. Juergen Siepmann, Ronald A. Siegel, and Michael J. Rathbone. Boston, MA: Springer US.  
<http://link.springer.com/10.1007/978-1-4614-0881-9> (April 2, 2020).

- [Su,04] Sung, H J, Carson M, Chad J, and Zorina S. G. 2004. "The Effect of Scaffold Degradation Rate on Three-Dimensional Cell Growth and Angiogenesis." *Biomaterials* 25(26): 5735–42.
- [Ta,12] Tabatabaei, F S. 2012. "Craniomaxillofacial Bone Engineering by Scaffolds Loaded with Stem Cells: A Systematic Review." *Journal of Dental School* 30(2): 113–30.
- [Ti,12] Tikhomirov, V. K. 2012. "Optimizing Er/Yb Ratio and Content in ErYb Co-Doped Glass-Ceramics for Enhancement of the up- and down-Conversion Luminescence." *Solar Energy Materials and Solar Cells* 100: 209–15.
- [Wi,06] Will, G. 2006. Powder Diffraction: The Rietveld Method and the Two Stage Method to Determine and Refine Crystal Structures from Powder Diffraction Data *Powder Diffraction: The Rietveld Method and the Two Stage Method to Determine and Refine Crystal Structures from Powder Diffraction Data*.
- [Wi,09] Williams, D F. 2009. "On the Nature of Biomaterials." *Biomaterials* 30(30): 5897–5909. [http://www.thelantern.com.au/resource\\_detail.php?id=266](http://www.thelantern.com.au/resource_detail.php?id=266) (April 2, 2020).
- [Ya,19] Yang, D. 2019. "Weakening Thermal Quenching to Enhance Luminescence of Er<sup>3+</sup> Doped  $\beta$ -NaYF<sub>4</sub> Nanocrystals via Acid-treatment." *Journal of the American Ceramic Society* 102(10): 6027–37. <https://onlinelibrary.wiley.com/doi/abs/10.1111/jace.16490> (March 24, 2020).
- [Ya,07] Yao, A. 2007. "In Vitro Bioactive Characteristics of Borate-Based Glasses with Controllable Degradation Behavior." *Journal of the American Ceramic Society* 90(1): 303–6. <http://doi.wiley.com/10.1111/j.1551-2916.2006.01358.x> (March 31, 2020).
- [Yi,91] Yie W, C. 1991. *Novel Drug Delivery Systems*. 2nd ed. ed. Chien Yie W. CRC Press.
- [Yl,00] Ylänen, H, Kaj H. K, Ari I, and Hannu T. A. 2000. "Effect of Immersion in SBF on Porous Bioactive Bodies Made by Sintering Bioactive Glass Microspheres." *Journal of Non-Crystalline Solids* 275(1): 107–15.
- [Yu,15] Yun, Y H, Byung K L, and Kinam P. 2015. "Controlled Drug Delivery: Historical Perspective for the next Generation." *Journal of Controlled Release* 219: 2–7. <https://linkinghub.elsevier.com/retrieve/pii/S0168365915301747> (April 2, 2020).
- [Zh,17] Zhang, B J. 2017. "Enhanced Osteogenesis of Multilayered Pore-Closed Microsphere-Immobilized Hydroxyapatite Scaffold: Via Sequential Delivery of Osteogenic Growth Peptide and BMP-2." *Journal of Materials Chemistry B* 5(41): 8238–53.
- [Zh,12] Zhang, D, Himanshu J, Hupa M, and Hupa L. 2012. "In-Vitro Degradation and Bioactivity of Tailored Amorphous Multi Porous Scaffold Structure" ed. A. Bandyopadhyay. *Journal of the American Ceramic Society* 95(9): 2687–94. <http://doi.wiley.com/10.1111/j.1551-2916.2012.05110.x> (March 31, 2020).